

Constraining extra fermion(s) from the Higgs boson data

G. Moreau

Laboratoire de Physique Théorique, Bâtiment 210, CNRS, Université Paris-sud 11, F-91405 Orsay Cedex, France

(Received 15 October 2012; published 24 January 2013)

First, we study the fit of the Higgs boson rates, based on all the latest collider data, in the effective framework for any extra fermion(s) (EF). The best-fit results are presented in a generic formalism allowing us to apply those for the test of any EF scenario under the assumption that the corrections to the Higgs couplings are coming exclusively from EF effects. The variations of the fit with each one of the five fundamental parameters are described, and the obtained fits can be better than in the Standard Model (SM). We show how the determination of the EF loop contributions to the Higgs couplings with photons and gluons is relying on the knowledge of the top and bottom Yukawa couplings (affected by EF mixings); for determining the latter coupling, the relevance of the investigation of the Higgs production in association with bottom quarks is emphasized. In the instructive approximation of a single EF, we find that the constraints from the fit already turn out to be quite predictive in both cases of an EF mixed or not with SM fermions, and especially when combined with the extra-quark (-lepton) mass bounds from direct EF searches at the LHC (LEP) collider. In the case of an unmixed extra quark (in the same color representation as SM quarks), nontrivial fit constraints are pointed out on the Yukawa couplings for masses up to ~ 200 TeV. In particular, we define the *extra dysfermiophilia*, which is predicted at 68.27% C.L. for any single extra quark (independently of its electric charge). Another result is that, among any components of SM multiplet extensions, the extra quark with a $-7/3$ electric charge is the one preferred by the present Higgs fit.

DOI: [10.1103/PhysRevD.87.015027](https://doi.org/10.1103/PhysRevD.87.015027)

PACS numbers: 14.65.Jk, 14.60.Hi, 14.80.Ec

I. INTRODUCTION

Recently, based on the combined LHC data collected at the center-of-mass energies of $\sqrt{s} = 7$ TeV and 8 TeV, the ATLAS [1] and CMS [2] Collaborations have independently announced the discovery at the $\sim 5\sigma$ level of a new resonance—with a mass close to 125 GeV—which can be identified as the missing Standard Model (SM) cornerstone: the Higgs boson [3–6]. The long list of measurements of the various Higgs boson rates provided during these last months by the two LHC collaborations [7,8] constitutes a new precious source of experimental results which can be exploited to test and constrain indirectly theories beyond the SM.

Most of the theories underlying the SM and addressing the gauge hierarchy problem predict the existence of new fermions, like charginos/neutralinos in supersymmetry, fermionic Kaluza-Klein (KK) excitations in higher-dimensional scenarios (e.g., gauge-Higgs unification frameworks as in Ref. [9] or the warped extra-dimension setup [10,11] with matter in the bulk [12–31]), excited resonances of bounded states in the dual composite Higgs [32–39] or composite top [40,41] models and top quark multiplet components in the little Higgs context [42–44]. Additional fermions could also arise as fourth generations [45] or as components embedded e.g., in simple SU(5) representations of gauge unification theories [46].

In the first part of this paper, we will combine all the Higgs rate measurements to constrain any model with extra

fermions (i.e., of any baryon/lepton number, Yukawa/gauge coupling) that are able to induce corrections to the Higgs couplings.¹ We will assume that the presence of an extra fermion(s) (EF) constitutes the only origin of significant deviations to the Higgs interactions. Note that our results also apply to any model with an extra scalar field (s) or vector boson(s) leading to significant Higgs interaction deviations, but not through their mixing(s) respectively with the Higgs boson or SM gauge bosons (cf. end of Sec. II B). By using a generic parametrization, we will determine the corrections to the Higgs couplings coming from fermion mixing or new loop-level exchanges, which are favored by the fits of the Higgs boson rates. We will show that the best Higgs rate fits obtained could be seen as first indirect indications of the presence of an EF since those fits can be better than the SM fit; another way of seeing this indication will be to observe that the best-fit regions for the EF-induced corrections to the Higgs couplings do not contain the vanishing-correction point (SM point).

In the second part of the paper, the Higgs fit constraints will be applied to characteristic and well-motivated classes of single EF scenarios (extra quark/lepton) and will reveal themselves to be already quite predictive. We will focus on single EFs in same color representations as

¹The extra fermions are assumed to be heavier than the Higgs field to avoid new Higgs decay openings (in particular, invisible decays into stable particles) that would require special treatments.

the SM quarks or leptons; various (including extreme) electric charges will be considered for the extra quark whereas the extra lepton will be assumed to have the same charge as the SM charged leptons.

Let us close the Introduction by comparing our analysis to the related literature. The constraints from Higgs rate fits on corrections to the Higgs couplings induced exclusively by EFs have been partly studied in analyses aimed at studying all the possible types of corrections [47–61] (see Ref. [62] for a statistical analysis by the ATLAS Collaboration). A first extension of the present work is to describe qualitatively and quantitatively the effect of varying the correction to the bottom-quark Yukawa coupling (parametrized here by c_b , the ratio of the bottom Yukawa coupling over its SM prediction) on constraints for other Higgs couplings; similarly, we study the dependence of the rate fit on c_τ , namely the ratio of the tau-lepton Yukawa coupling over its SM value (without the simplifying assumption $c_\tau = c_b$). Another extension is the inclusion of the data on the Higgs production in association with a top-quark pair (relying on the top ratio c_t) and on the Higgs decay channel $h \rightarrow \bar{\tau}\tau$ (involving c_τ) which can play a role in constraining fermion mixings. Because of the inclusion of the former data, we do not integrate out the top quark which allows us to explicitly study the c_t parameter (and we do not take e.g., $c_t = c_b$): we point out in particular that the c_t variation leads to simple translations of the best-fit domains obtained.

Let us note that our fits are performed over the three free parameters c_b , c_{gg} and $c_{\gamma\gamma}$ (related to the hgg and $h\gamma\gamma$ coupling corrections defined later) for characteristic fixed values of c_τ and c_t .² In a second step, we fix c_b for studying examples of EF scenarios.

In Sec. II, we discuss the theoretical context and the formalism used. Then the measurements of the Higgs boson rates are summarized in Sec. III and confronted to the parameter space of EF scenarios in Sec. IV. In Sec. IVA we describe the fit procedure and in Sec. IVB we present the numerical results while in Sec. IV C we study the simplified case of a unique EF. We conclude in Sec. V.

II. THEORETICAL FRAMEWORK

A. The physical context

We consider the general framework with any EF able to modify the Higgs couplings. In our context, no other source of physics beyond the SM is responsible for deviations of the Higgs couplings; this choice allows one to concentrate one's efforts on the class of models with EFs and in turn to have a deeper analysis of the parameter

²In order to explain clearly the influences of these five relevant parameters on the Higgs rate fit, we do not marginalize any of those parameters.

space. In particular, we assume the Higgs scalar field to receive no coupling modifications due to significant mixings with other scalars as it can occur e.g., in extended Higgs sectors.

For example, such a framework could be realized concretely in warped extra-dimension scenarios where some so-called custodians (fermionic KK modes) [63–74] would be below the TeV scale inducing e.g., large top mixings, while the decoupling KK gauge boson excitations would be much above ~ 3 TeV (the order of the lower bound from electroweak (EW) precision tests [63,75,76]) forbidding in particular significant corrections to the Higgs couplings with gauge bosons.

From a more basic point of view, in a bottom-up approach without prejudice, this hypothesis that EFs mainly affect the Higgs observables is one simple possibility, among others, to be considered. This possibility has been considered for instance in Refs. [77–84] where the sole effects from some EF species—namely the vectorlike fermions (which can arise in many SM extensions)—on the Higgs production cross sections and branching ratios were considered.

In a different context from this, other sources of large Higgs coupling deviations could exist as well—like extra bosons below ~ 10 TeV that could be needed e.g., in an UV completion theory allowing a vacuum stability in the presence of new fermions at the EW energy scale with large Yukawa couplings [85]. Then the present results might be used to understand specifically the impact of EFs on the Higgs rate fits.

Since we adopt a generic approach, we will not make assumptions in particular regarding the EF representations under the $SU(2)_L$ gauge group. Hence it will not be possible to study EW precision tests on EFs as those tests depend on the $SU(2)_L$ isospins of EFs. Such tests can be performed once a given EF model is chosen, like for instance in Refs. [79–81,86] where it was shown that some EF models can pass the EW constraints.

B. The effective Lagrangian

In our framework, all the Higgs couplings receiving corrections can be written in the following effective Lagrangian, which allows us to work out the current Higgs phenomenology at the LHC and the Tevatron collider:

$$\begin{aligned} \mathcal{L}_h = & -c_t Y_t h \bar{t}_L t_R - c_b Y_b h \bar{b}_L b_R - c_\tau Y_\tau h \bar{\tau}_L \tau_R \\ & + C_{h\gamma\gamma} \frac{\alpha}{\pi v} h F^{\mu\nu} F_{\mu\nu} + C_{hgg} \frac{\alpha_s}{12\pi v} h G^{a\mu\nu} G_{\mu\nu}^a \\ & + \text{H.c.}, \end{aligned} \quad (1)$$

where $Y_{t,b,\tau}$ are the SM Yukawa coupling constants of the associated fermions in the mass eigenbasis, v is the Higgs

vacuum expectation value, the subscripts L/R indicate the fermion chirality and the tensor fields in the $h\gamma\gamma$ and hgg coupling terms (following e.g., the normalization adopted in Ref. [59]) are respectively the electromagnetic and gluon field strengths. The $c_{t,b,\tau}$ parameters taken real for simplicity are defined such that the limiting case $c_{t,b,\tau} \rightarrow 1$ corresponds to the SM; deviations from unity of those parameters can be caused by mixings of EFs (like t' states, etc.) with the SM fermions. Only the Yukawa couplings of the third generation are supposed to receive potentially important corrections from EF mixing effects since EFs are closer in mass to the third generation and this heavy generation is in general more intimately connected to the ultraviolet physics, like the top quark in warped/composite frameworks.

A few remarks are in order regarding the terms absent from the Lagrangian (1). First, we only consider tree-level (loop-level) corrections to couplings induced at the tree level (loop level) in the SM, i.e., we calculate exclusively the dominant corrections. In the absence of a tree-level correction from EF origins for a certain SM tree-level induced coupling, we do not go to the next order so that the global analysis coherence is preserved. Secondly, we have not included in the Lagrangian the $hZ\gamma$ coupling [87] as it is not constrained by a dedicated experimental analysis e.g., in the $Z\gamma$ channel, and the EF-induced corrections to the relatively small $\Gamma(h \rightarrow Z\gamma)$ width are expected to be too weak to change significantly the total Higgs width (involved in all branching fractions). For similar reasons, we have not considered flavor-changing Yukawa couplings (those are not excluded in some EF scenarios and could induce new partial Higgs decay widths).

Let us make another comment about the Lagrangian (1). Neglecting the mixings with the first two SM flavors, one gets $-Y_{t,b,\tau} = m_{t,b,\tau}/v$ [the minus sign is due to the sign taken in front of the Yukawa couplings in Eq. (1)], where $m_{t,b,\tau}$ are the final masses generated after EW symmetry breaking. The EF mixing effect on the Yukawa couplings enters via the $c_{t,b,\tau}$ parameters. These parameter values also contain the 3×3 SM flavor mixing effect in case it is not neglected. This 3×3 mixing is considerable in the lepton sector (while Cabibbo-Kobayashi-Maskawa mixing angles [88] are typically small) but there is a possibility is that the strongest mixing angles originate from the neutrino mass matrix. Now even if a Higgs decay channel into neutrinos is open, like in the simple case of added right-handed neutrino singlets leading to neutrino Yukawa couplings, the partial width into neutrinos would typically be so tiny compared to others—even for huge neutrino Yukawa coupling enhancements by say 2 orders of magnitude—that it would not affect the Higgs fit analysis.

Summing over the dominant loop contributions, the coefficients of the dimension-five operators in Eq. (1) can be written as

$$C_{hgg} = 2C(t)A[\tau(m_t)](c_t + c_{gg}) + 2C(b)A[\tau(m_b)]c_b + 2C(c)A[\tau(m_c)], \quad (2)$$

$$C_{h\gamma\gamma} = \frac{N_c^t}{6} Q_f^2 A[\tau(m_t)](c_t + c_{\gamma\gamma}) + \frac{N_c^b}{6} Q_f^2 A[\tau(m_b)]c_b + \frac{N_c^c}{6} Q_f^2 A[\tau(m_c)] + \frac{N_c^\tau}{6} Q_f^2 A[\tau(m_\tau)]c_\tau + \frac{1}{8} A_1[\tau(m_W)], \quad (3)$$

where m_c (m_W) is the charm quark (W^\pm boson) mass, $C(r)$ is defined for the color representation, r , by $\text{Tr}(T_r^a T_r^b) = C(r)\delta^{ab}$ [T^a denoting the eight generators of $SU(3)_c$], N_c^f is the number of colors for the fermion f , Q_f is the electromagnetic charge for f , $A[\tau(m)]$ and $A_1[\tau(m)]$ are respectively the form factors for spin 1/2 and spin 1 particles [87,89] normalized such that $A[\tau(m) \ll 1] \rightarrow 1$ and $A_1[\tau(m) \ll 1] \rightarrow -7$ with $\tau(m) = m_h^2/4m^2$ (for $m_h \simeq 125$ GeV one has $A_1[\tau(m_W)] \simeq -8.3$ whereas $A[\tau(m > 600 \text{ GeV})] \simeq 1.0$). The terms proportional to c_t , c_b and c_τ account for the contributions from the fermionic triangular loops involving respectively the top, bottom quark and tau lepton Yukawa coupling. The $A[\tau(m_c)]$ and $A_1[\tau(m_W)]$ terms are for the SM loop exchanges of the charm quark and W^\pm boson. The dimensionless c_{gg} and $c_{\gamma\gamma}$ quantities vanishing in the SM parametrize the EF loop-exchange contributions to the hgg and $h\gamma\gamma$ couplings. This choice of parametrization in Eq. (2) with a common factor in front of c_t and c_{gg} [as well as for c_t and $c_{\gamma\gamma}$ in Eq. (3)] makes easier the understanding of the c_t influence on the best-fit c_{gg} (or $c_{\gamma\gamma}$) ranges that will be discussed in Sec. IV B.

Note also that an extra scalar field(s) unmixed with the Higgs boson h (like a squark in supersymmetry) or an extra vector boson(s) unmixed with the SM gauge bosons could affect the Higgs couplings only through new loop contributions to the c_{gg} and $c_{\gamma\gamma}$ quantities studied here.

C. Higgs rate modifications

Within the present context, let us write explicitly certain Higgs rates normalized to their SM prediction, which will prove to be useful in the following. The expression for the cross section of the gluon-gluon fusion mechanism of single Higgs production over its SM prediction reads as (for the LHC or Tevatron)

$$\frac{\sigma_{gg \rightarrow h}}{\sigma_{gg \rightarrow h}^{\text{SM}}} \simeq \frac{[(c_t + c_{gg})A[\tau(m_t)] + c_b A[\tau(m_b)] + A[\tau(m_c)]]^2}{[A[\tau(m_t)] + A[\tau(m_b)] + A[\tau(m_c)]]^2}. \quad (4)$$

The expression for the ratio of the diphoton partial decay width over the SM expectation is

$$\frac{\Gamma_{h \rightarrow \gamma\gamma}}{\Gamma_{h \rightarrow \gamma\gamma}^{\text{SM}}} \simeq \frac{|\frac{1}{4}A_1[\tau(m_W)] + (\frac{2}{3})^2(c_t + c_{\gamma\gamma})A[\tau(m_t)] + (-\frac{1}{3})^2c_bA[\tau(m_b)] + (\frac{2}{3})^2A[\tau(m_c)] + \frac{1}{3}c_\tau A[\tau(m_\tau)]|^2}{|\frac{1}{4}A_1[\tau(m_W)] + (\frac{2}{3})^2A[\tau(m_t)] + (-\frac{1}{3})^2A[\tau(m_b)] + (\frac{2}{3})^2A[\tau(m_c)] + \frac{1}{3}A[\tau(m_\tau)]|^2}. \quad (5)$$

The ratios for the partial decay widths into the bottom quark and tau lepton pairs as well as for the cross section of Higgs production in association with a top pair (LHC or Tevatron) are given by

$$\frac{\Gamma_{h \rightarrow \bar{b}b}}{\Gamma_{h \rightarrow \bar{b}b}^{\text{SM}}} \simeq |c_b|^2, \quad \frac{\Gamma_{h \rightarrow \bar{\tau}\tau}}{\Gamma_{h \rightarrow \bar{\tau}\tau}^{\text{SM}}} \simeq |c_\tau|^2, \quad \frac{\sigma_{\text{hit}}}{\sigma_{\text{hit}}^{\text{SM}}} \simeq |c_t|^2. \quad (6)$$

Let us make a comment related to the mass insertion in the triangular loops of fermions inducing the $h\gamma\gamma$ and hg couplings. Strictly speaking, a factor ϵ_t equal to the ratio of the sign of m_t in the SM over sign (m_t) in the EF scenario should multiply c_t in Eqs. (2) and (3) or Eqs. (4) and (5) (similarly for $\epsilon_b c_b$ and $\epsilon_\tau c_\tau$); in other words, if for instance $\epsilon_t = -1$ the values for c_t obtained below would have to be interpreted instead as values for $-c_t$ [the observables of Eq. (6) being insensitive to the $c_{t,b,\tau}$ signs].

D. Ratio of $c_{\gamma\gamma}$ and c_{gg}

For a better understanding of the above parametrization, we finally provide the examples of expressions for the c_{gg} and $c_{\gamma\gamma}$ quantities, in the case of the existence of a t' quark (same color number and electromagnetic charge as the top; possibly vectorlike as e.g., in Refs. [90,91]), an exotic $q_{5/3}$ quark with electromagnetic charge 5/3 and an additional ℓ' lepton (colorless), in terms of their physical Yukawa couplings and mass eigenvalues:

$$c_{gg} = \frac{1}{C(t)A[\tau(m_t)]/v} \left[-C(t') \frac{Y_{t'}}{m_{t'}} A[\tau(m_{t'})] - C(q_{5/3}) \frac{Y_{q_{5/3}}}{m_{q_{5/3}}} A[\tau(m_{q_{5/3}})] + \dots \right], \quad (7)$$

$$c_{\gamma\gamma} = \frac{1}{N_c Q_t^2 A[\tau(m_t)]/v} \left[-3 \left(\frac{2}{3}\right)^2 \frac{Y_{t'}}{m_{t'}} A[\tau(m_{t'})] - N_c^{q_{5/3}} \left(\frac{5}{3}\right)^2 \frac{Y_{q_{5/3}}}{m_{q_{5/3}}} A[\tau(m_{q_{5/3}})] - Q_{\ell'}^2 \frac{Y_{\ell'}}{m_{\ell'}} A[\tau(m_{\ell'})] + \dots \right]. \quad (8)$$

The dots stand for any other EF loop contributions. The mass assumption made in Footnote ¹ leads to real $A[\tau(m_{f'})]$ functions and thus real c_{gg} , $c_{\gamma\gamma}$ values for real masses and Yukawa coupling constants, as appears clearly in the two above expressions.

It will turn out to be instructive to express the ratio of these parameters in the simplified scenario where a new single q' quark is affecting the Higgs couplings. Denoting its electromagnetic charge as $Q_{q'}$ and assuming the q' to have the same color representation as the top quark, this ratio reads as

$$\frac{c_{\gamma\gamma}}{c_{gg}} \Big|_{q'} = \frac{Q_{q'}^2}{(2/3)^2}. \quad (9)$$

This ratio takes indeed a simple form that will be exploited in Sec. IV C. In particular, notice that $c_{\gamma\gamma}|_{t'} = c_{gg}|_{t'}$. Clearly, q' should have nonvanishing Yukawa couplings to satisfy Eq. (9), otherwise $c_{\gamma\gamma}|_{q'} = c_{gg}|_{q'} = 0$. In the specific case of a vectorlike $q'_{L/R}$, this one could for example constitute a singlet under the $SU(2)_L$ gauge group and have a Yukawa coupling with another $q''_{R/L}$ state of same $Q_{q'}$ charge but embedded in a $SU(2)_L$ doublet. Then the heaviest $q_{L/R}^{(2)}$ mass eigenstate composed of $q'_{L/R}$ and $q''_{L/R}$ could decouple from the Higgs sector so that the orthogonal $q_{L/R}^{(1)}$ composition would represent the considered unique new quark influencing significantly the Higgs couplings.

III. THE HIGGS BOSON DATA

All the Higgs rates which have been measured at the Tevatron and LHC (for $\sqrt{s} = 7$ and 8 TeV) are defined in this section. The references with their latest experimental values are also given below (these values have been summarized in Ref. [58]).

Generically, the measured observables are the signal strengths whose theoretical predictions read as (in the narrow width approximation as used in Ref. [62])

$$\mu_{s,c,i}^p \simeq \frac{\sigma_{\text{gg} \rightarrow \text{h}}|_s + \frac{\epsilon_{\text{hq}}}{\epsilon_{\text{gg} \rightarrow \text{h}}} |_{s,c,i}^p \sigma_{\text{hq}}^{\text{SM}}|_s + \frac{\epsilon_{\text{hv}}}{\epsilon_{\text{gg} \rightarrow \text{h}}} |_{s,c,i}^p \sigma_{\text{hv}}^{\text{SM}}|_s + \frac{\epsilon_{\text{ht}}}{\epsilon_{\text{gg} \rightarrow \text{h}}} |_{s,c,i}^p \sigma_{\text{ht}}|_s}{\sigma_{\text{gg} \rightarrow \text{h}}^{\text{SM}}|_s + \frac{\epsilon_{\text{hq}}}{\epsilon_{\text{gg} \rightarrow \text{h}}} |_{s,c,i}^p \sigma_{\text{hq}}^{\text{SM}}|_s + \frac{\epsilon_{\text{hv}}}{\epsilon_{\text{gg} \rightarrow \text{h}}} |_{s,c,i}^p \sigma_{\text{hv}}^{\text{SM}}|_s + \frac{\epsilon_{\text{ht}}}{\epsilon_{\text{gg} \rightarrow \text{h}}} |_{s,c,i}^p \sigma_{\text{ht}}^{\text{SM}}|_s} B_{\text{h} \rightarrow \text{XX}}, \quad \text{with} \quad \sigma_{\text{gg} \rightarrow \text{h}}|_s = \frac{\sigma_{\text{gg} \rightarrow \text{h}}}{\sigma_{\text{gg} \rightarrow \text{h}}^{\text{SM}}} \sigma_{\text{gg} \rightarrow \text{h}}^{\text{SM}}|_s, \\ \sigma_{\text{hit}}|_s = \frac{\sigma_{\text{hit}}}{\sigma_{\text{hit}}^{\text{SM}}} \sigma_{\text{hit}}^{\text{SM}}|_s, \quad \Gamma_{\text{h} \rightarrow \gamma\gamma} = \frac{\Gamma_{\text{h} \rightarrow \gamma\gamma}}{\Gamma_{\text{h} \rightarrow \gamma\gamma}^{\text{SM}}} \Gamma_{\text{h} \rightarrow \gamma\gamma}^{\text{SM}}, \quad \Gamma_{\text{h} \rightarrow \bar{b}b} = \frac{\Gamma_{\text{h} \rightarrow \bar{b}b}}{\Gamma_{\text{h} \rightarrow \bar{b}b}^{\text{SM}}} \Gamma_{\text{h} \rightarrow \bar{b}b}^{\text{SM}}, \quad \Gamma_{\text{h} \rightarrow \bar{\tau}\tau} = \frac{\Gamma_{\text{h} \rightarrow \bar{\tau}\tau}}{\Gamma_{\text{h} \rightarrow \bar{\tau}\tau}^{\text{SM}}} \Gamma_{\text{h} \rightarrow \bar{\tau}\tau}^{\text{SM}}, \quad (10)$$

where the p exponent labels the Higgs channel defined by its production and decay processes, the s subscript represents the squared of the energy (we will note $\sqrt{s} = 1.96, 7, 8$ in TeV) of the realized measurement, the c subscript stands for the experimental collaboration (CDF and D0 at the Tevatron, ATLAS or CMS at the LHC) having performed the measurement and i is an integer indicating the event cut category considered. $\sigma_{\text{h}q\bar{q}}$ is the predicted cross section for the Higgs production in association with a pair of light SM quarks and $\sigma_{\text{h}V}$ is for the production in association with a gauge boson ($V \equiv Z^0, W^\pm$ bosons); their s subscript indicates the energy and in turn which collider is considered. The $B_{\text{h} \rightarrow \text{XX}}$ (X stands for any possible final state particle) are the branching ratios defined from all the opened Higgs decay widths which are modified according to the second line of Eq. (10) and taken as in the SM for the others. The SM rates at the LHC for a given energy like $\sigma_{\text{gg} \rightarrow \text{h}}^{\text{SM}}|_s$ and the SM partial widths $\Gamma_{\text{h} \rightarrow \text{XX}}^{\text{SM}}$ are taken from Ref. [92] (including the cross section corrections at next-to-next-to-leading order in QCD and next-to-leading order in the EW sector except for $\sigma_{\text{h}t\bar{t}}^{\text{SM}}$ at next-to-leading order in QCD), while the SM rates at the Tevatron are from Ref. [93] (QCD corrections at next-to-next-to-leading order). The cross section and partial width ratios in the second line of Eq. (10) are those in the considered effective theory with EFs expressed in Eqs. (4)–(6). The EW/QCD corrections are expected typically to be compensated in these ratios (especially for heavy EFs in the same gauge group representation as the SM fermions). Finally, $\epsilon_{\text{gg} \rightarrow \text{h}}$ for the $\text{gg} \rightarrow \text{h}$ reaction example is the experimental efficiency (detector acceptance, particle identification, isolation, etc.) including the (kinematical) selection cut effects; the efficiency ratios entering Eq. (10) are obtained by multiplying the SM cross section ratios by the ratios of expected Higgs reaction compositions (in %) derived via simulations and provided in the relevant experimental papers (see just below). These selection efficiencies relying on the Higgs mass are identical in the SM and in EF frameworks (i.e., in the denominator and numerator of $\mu_{s,c,i}^p$). Here is the list of Higgs channels that have been experimentally investigated (corresponding, once summed, to 55 measured signal strengths).

- (i) For the process I , $\text{pp} \rightarrow \text{h}, \text{h} \rightarrow \gamma\gamma$, the Higgs field is mainly produced by the gluon-gluon fusion; the signal strengths $\mu_{7/8,\text{ATLAS/CMS},i}^I$ are proportional to $B_{\text{h} \rightarrow \gamma\gamma}$ and depend on the efficiency ratios like e.g., $\epsilon_{\text{h}q\bar{q}}/\epsilon_{\text{gg} \rightarrow \text{h}}|_{7/8,\text{ATLAS/CMS},i}^I$ which can be derived from the reaction compositions provided in Ref. [94] (ATLAS) and Ref. [95] updated by Ref. [96] (CMS). While for ATLAS, nine cut categories ($i = 1, \dots, 9$) have been applied on the data collected at $\sqrt{s} = 7$ TeV in 2011 (4.8 fb^{-1}) and 8 TeV in 2012 (5.8 fb^{-1}), leading to a measured mass $m_h \simeq 126.0$ GeV after combination with other channels [97]. CMS has chosen four cut classes

($j = 0, \dots, 3$) to treat the 2011 (5.1 fb^{-1}) and 2012 (5.3 fb^{-1}) data, pointing out a mass $m_h \simeq 125.3$ GeV from combination with the ZZ channel. Note that in Eq. (10), the terms

$$\frac{\epsilon_{\text{h}Z}}{\epsilon_{\text{gg} \rightarrow \text{h}}}|_{7/8,\text{ATLAS},i}^I \sigma_{\text{h}Z}^{\text{SM}}|_{7/8} + \frac{\epsilon_{\text{h}W}}{\epsilon_{\text{gg} \rightarrow \text{h}}}|_{7/8,\text{ATLAS},i}^I \sigma_{\text{h}W}^{\text{SM}}|_{7/8},$$

for the ATLAS data must be replaced by $(\epsilon_{\text{h}Z+\text{h}W}/\epsilon_{\text{gg} \rightarrow \text{h}}|_{7/8,\text{CMS},j}^I)(\sigma_{\text{h}Z}^{\text{SM}} + \sigma_{\text{h}W}^{\text{SM}})|_{7/8}$ for CMS (a common efficiency is set).

- (ii) In the diphoton channel, other series of cuts have been employed to increase the vector boson fusion contribution $\text{pp} \rightarrow \text{h}q\bar{q}, \text{h} \rightarrow \gamma\gamma$ defining the process noted II . The signal strengths $\mu_{7/8,\text{ATLAS/CMS},i}^{II}$ rely on the efficiency ratios obtained from the reaction compositions in Refs. [94–96]. A unique cut category is selected by ATLAS to tag the dijet final state, whereas two of them ($i \equiv \text{tight, loose}$) are used with the CMS data at $\sqrt{s} = 8$ TeV.
- (iii) The last diphoton channel analyzed, process III , is the inclusive Higgs production at the Tevatron $\text{p}\bar{\text{p}} \rightarrow \text{h}, \text{h} \rightarrow \gamma\gamma$. The $\mu_{1.96,\text{CDF+D0}}^{III}$ strength is simply fixed by $\epsilon/\epsilon_{\text{gg} \rightarrow \text{h}}|_{1.96,\text{CDF+D0}}^{III} \simeq 1$ [93] for each Higgs production cross section in Eq. (10).
- (iv) For the process IV , $\text{pp} \rightarrow \text{h}V[\text{h} \rightarrow \text{leptons}], \text{h} \rightarrow \bar{\text{b}}\text{b}$, all selection efficiencies vanish except $\epsilon_{\text{h}V}|_{7/8,\text{ATLAS/CMS}}^{IV} \simeq 1$ [97–99] [of course in such a case, one should not divide by $\epsilon_{\text{gg} \rightarrow \text{h}}$ in Eq. (10)] so that $\mu_{7/8,\text{ATLAS/CMS}}^{IV} \simeq B_{\text{h} \rightarrow \bar{\text{b}}\text{b}}/B_{\text{h} \rightarrow \bar{\text{b}}\text{b}}^{\text{SM}}$, since $\sigma_{\text{h}V}^{\text{SM}}$ does not receive corrections in the EF framework.
- (v) Similarly, for the process V , $\text{p}\bar{\text{p}} \rightarrow \text{h}V[\text{h} \rightarrow \text{leptons}], \text{h} \rightarrow \bar{\text{b}}\text{b}$, one has $\mu_{1.96,\text{CDF+D0}}^V = \mu_{7/8,\text{ATLAS/CMS}}^{IV}$ [93].
- (vi) The process VI , $\text{pp} \rightarrow \text{h}t\bar{t}, \text{h} \rightarrow \bar{\text{b}}\text{b}$, is characterized by vanishing efficiencies except $\epsilon_{\text{h}t\bar{t}}|_{7,\text{CMS}}^{VI} \simeq 1$ leading to

$$\mu_{7,\text{CMS}}^{VI} \simeq \frac{\sigma_{\text{h}t\bar{t}}}{\sigma_{\text{h}t\bar{t}}^{\text{SM}}} \frac{B_{\text{h} \rightarrow \bar{\text{b}}\text{b}}}{B_{\text{h} \rightarrow \bar{\text{b}}\text{b}}^{\text{SM}}}. \quad (11)$$

The experimental value, which will be mentioned in the next section, is $\mu_{7,\text{CMS}}^{VI}|_{\text{exp}} = -0.75_{-1.8}^{+2}$ [99].

- (vii) The reaction VII , $\text{pp} \rightarrow \text{h}, \text{h} \rightarrow ZZ$, has a strength $\mu_{7/8,\text{ATLAS/CMS}}^{VII}$ calculated according to selection efficiencies all equal to unity (for CMS see Ref. [99] and for ATLAS Ref. [100] at $\sqrt{s} = 7$ TeV or Ref. [97] at 8 TeV).
- (viii) In the same way, for the reaction $VIII$, $\text{pp} \rightarrow \text{h}, \text{h} \rightarrow \text{WW}$, the strength $\mu_{7/8,\text{ATLAS}}^{VIII}$ is computed with efficiencies at unity (see Ref. [98] for 7 TeV and Ref. [101] for 8 TeV, both updated by

Ref. [97]), whereas $\mu_{7/8,\text{CMS}}^{\text{VIII}}$ is based on vanishing efficiencies except $\epsilon_{\text{gg}\rightarrow\text{h}}^{\text{VIII}}|_{7/8,\text{CMS}} \simeq 1$ [99].

- (ix) From analog considerations as in the channel IV, one predicts $\mu_{7/8,\text{CMS}}^{\text{IX}} \simeq \mu_{7,\text{CMS}}^{\text{X}} \simeq B_{\text{h}\rightarrow\text{WW}}/B_{\text{h}\rightarrow\text{WW}}^{\text{SM}}$ for the processes IX, $\text{pp} \rightarrow \text{hqq}$, $\text{h} \rightarrow \text{WW}$, and X, $\text{pp} \rightarrow \text{hV}$, $\text{h} \rightarrow \text{WW}$ [99].
- (x) The channel XI, $\text{p}\bar{\text{p}} \rightarrow \text{h}$, $\text{h} \rightarrow \text{WW}$, has a strength $\mu_{1.96,\text{CDF+D0}}^{\text{XI}}$ containing exclusively efficiencies at unity [93].
- (xi) As in channel IV, one has the theoretical predictions $\mu_{7/8,\text{CMS}}^{\text{XII}} \simeq \mu_{7,\text{CMS}}^{\text{XIII}} \simeq B_{\text{h}\rightarrow\bar{\tau}\tau}/B_{\text{h}\rightarrow\bar{\tau}\tau}^{\text{SM}}$ for the processes XII, $\text{pp} \rightarrow \text{hqq}$, $\text{h} \rightarrow \bar{\tau}\tau$, and XIII, $\text{pp} \rightarrow \text{hV}$, $\text{h} \rightarrow \bar{\tau}\tau$ [99].
- (xii) Finally, for the process XIV, $\text{pp} \rightarrow \text{h}$, $\text{h} \rightarrow \bar{\tau}\tau$, the strength $\mu_{7,\text{ATLAS}}^{\text{XIV}}$ has the efficiencies equal to 1 [97,98] and $\mu_{7/8,\text{CMS}}^{\text{XIV}}$ has all efficiencies equal to zero but $\epsilon_{\text{gg}\rightarrow\text{h}}^{\text{XIV}}|_{7/8,\text{CMS}} \simeq 1$ [99].

IV. THE HIGGS RATE FITS

A. The fit procedure

In order to analyze the fit of the Higgs boson data from colliders within the effective theory described above, we assume Gaussian error statistics and we use the χ^2 function

$$\chi^2 = \sum_{p,s,c,i} \frac{(\mu_{s,c,i}^p - \mu_{s,c,i}^p|_{\text{exp}})^2}{(\delta\mu_{s,c,i}^p)^2}, \quad (12)$$

where the sum is taken over all the different channel observables defined in Sec. III and $\mu_{s,c,i}^p|_{\text{exp}}$ are the measured central values for the corresponding signal strengths. $\delta\mu_{s,c,i}^p$ are the uncertainties on these values and are obtained by symmetrizing the provided errors below and above the central values: $(\delta\mu_{s,c,i}^p)^2 = [(\delta\mu_{s,c,i}^p|^{+})^2 + (\delta\mu_{s,c,i}^p|^{-})^2]/2$. $\mu_{s,c,i}^p|_{\text{exp}}$ and $\delta\mu_{s,c,i}^p|^{\pm}$ are given in the experimental papers listed in Sec. III which contain the QCD error estimations.

The summation over all the signal strengths in Eq. (12) allows us to compare the maximum of available experimental information with the theoretical predictions in order to optimize the test of the effective EF theory. Note that the i subscript in this summation corresponds to exclusive cut categories into which the event samples are split.

The global fit is performed without including the correlation coefficient effects which are currently not supplied in the experimental papers. Nevertheless, this does not affect the statistical and uncorrelated systematic errors.

B. Fits in the $\{c_{gg}, c_{\gamma\gamma}, c_b\}$ space

In Eq. (12), $\chi^2 = \chi^2(c_t, c_b, c_\tau, c_{gg}, c_{\gamma\gamma})$ depends on the five effective parameters c_t , c_b , c_τ , c_{gg} , $c_{\gamma\gamma}$ through Eqs. (10) and (4)–(6). *A priori*, the fit analysis should be

performed over these five free parameters but to still be able to draw plots of the whole parameter space (and in turn study it graphically), one has to restrict it to a three-dimensional space. In this section, we will indeed choose three freely varying parameters c_{gg} , $c_{\gamma\gamma}$, c_b , and search for the best-fit regions in this three-dimensional space. Then we will show slices of these regions at several chosen values of c_b (i.e., in the plane $c_{\gamma\gamma}$ versus c_{gg}). This will be repeated for different fixed values of c_t and c_τ .

The motivation for fixing c_t and c_τ among the five effective parameters is the following. First, the $|c_\tau|$ range compatible at 1σ with the Higgs data is known and turns out to be roughly (0; ~ 1.8) (for $c_t \simeq 1$ and reasonable c_b values described later on) because the measured values for $\mu_{7/8,\text{CMS}}^{\text{XII}}$ are negative—even with the errors—so that $B_{\text{h}\rightarrow\bar{\tau}\tau}$, and in turn $\Gamma_{\text{h}\rightarrow\bar{\tau}\tau}$ and $|c_\tau|$, cannot be too large. Hence, there is no need to apply the numerical global fit analysis on c_τ , then treated as a free parameter, to find its relevant range. Secondly, for the purpose of demonstrating the c_t peculiarity (correlation with c_{gg} , $c_{\gamma\gamma}$) discussed in Sec. IV B 5, it is easier to choose ourselves its fixed values than to have those values dictated by the numerical best-fit search method.

So now, having the three free parameters c_{gg} , $c_{\gamma\gamma}$, c_b , we will show the best-fit domains in this three-dimensional space at 68.27% C.L. (1σ), 95.45% C.L. (2σ) and 99.73% C.L. (3σ) which correspond to established values of $\Delta\chi^2 = \chi^2 - \chi_{\text{min}}^2$ (χ_{min}^2 being the minimum χ^2 value reached in the $\{c_{gg}, c_{\gamma\gamma}, c_b\}$ space) (see for instance Ref. [88]).

In Fig. 1, we present four slices of these three-dimensional best-fit regions at four c_b values [$c_b = 0.75$ (a), 1 (b), 2.08 (c), 10 (d)] in the plane $c_{\gamma\gamma}$ versus c_{gg} . These regions are shown for three different fixed values of c_t but for the unique choice $c_\tau = 1$. The c_τ parameter is varied in the plots of Fig. 2 (again for three c_t values) where the behavior of the domain slice at $c_b = 2.08$ is still shown in the $\{c_{\gamma\gamma}, c_{gg}\}$ plane. Note that Fig. 1(c) has also been included in Fig. 2 [see plot (b)] for an easier comparison with Figs. 2(a) and 2(c). All plots of Figs. 1 and 2 are discussed in the following subsections.

1. The c ranges

A few comments are in order with respect to the reasonable choice of parameter ranges in Figs. 1 and 2. The naive perturbativity condition $|c_t Y_t| \leq 4\pi$ leads to $|c_t| \leq 18$ since $|Y_t| \simeq |m_t/v|$. The similar theoretical constraints for $|c_b|$ and $|c_\tau|$ are even less stringent due to the smaller $m_{b,\tau}$ values. The perturbativity considerations on $c_{\gamma\gamma}$ and c_{gg} are model dependent; for example, in the case of a t' state with $m_{t'}$ of the order of m_t , Eqs. (7) and (8) show that $c_{\gamma\gamma}$ and c_{gg} would typically set the t' Yukawa coupling (relatively to Y_t) and would thus have to satisfy roughly the same condition as c_t : $|c_{\gamma\gamma}| \leq 18$, $|c_{gg}| \leq 18$.

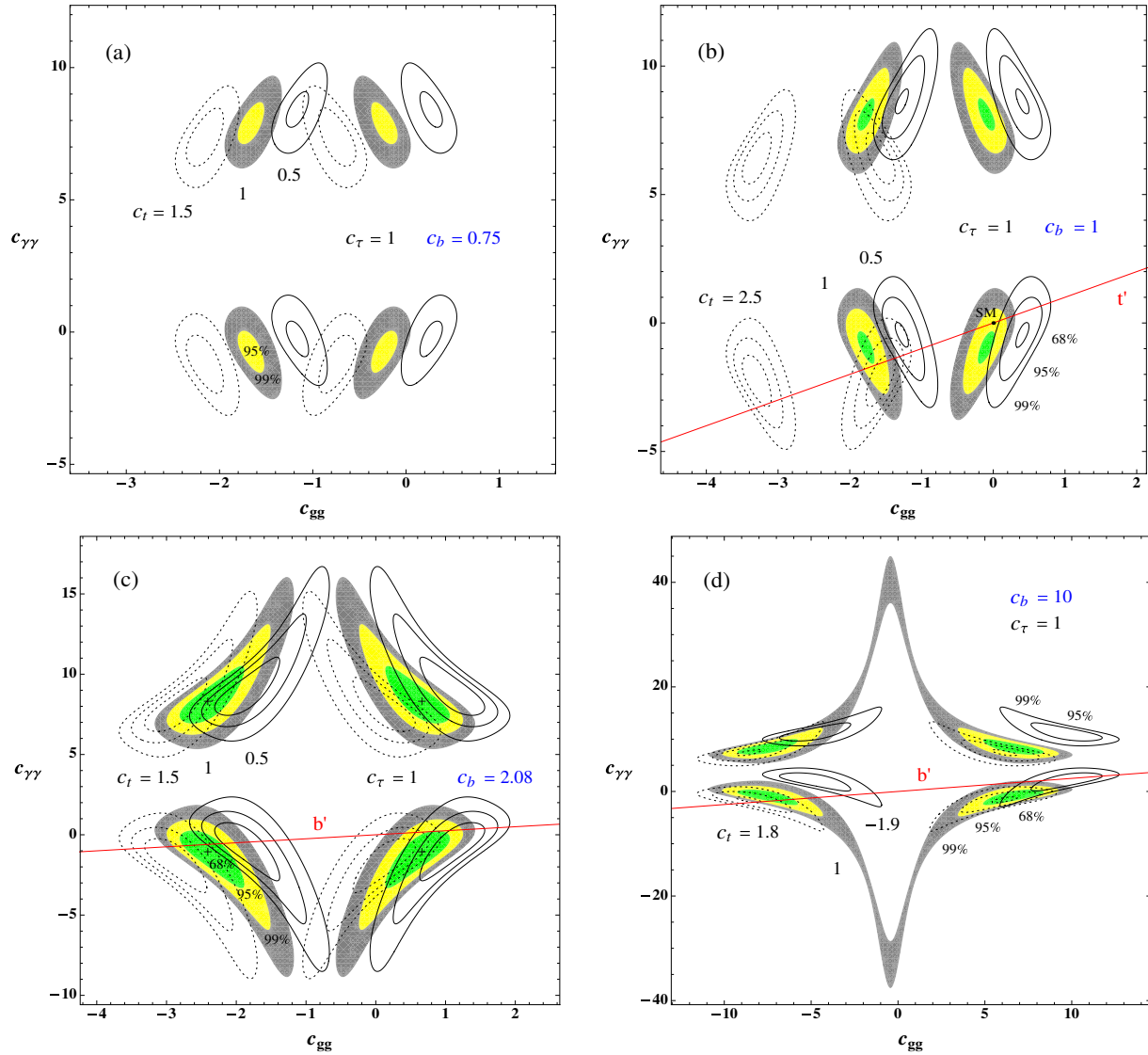


FIG. 1 (color online). Best-fit regions at 68.27% C.L. (green), 95.45% C.L. (yellow) and 99.73% C.L. (grey) in the plane $c_{\gamma\gamma}$ versus c_{gg} , for $c_\tau = 1$. Each one of the four figures (a, b, c, d) is associated to a certain c_b value written (blue) on the figure itself. In each figure, the regions are drawn for three c_t values, the corresponding value being indicated nearby the relevant region; the regions for the lowest, intermediate and highest c_t values are respectively shown by the plain contours, colored filled domains and dotted contours. The SM (black) point at $c_t = c_b = c_\tau = 1$, $c_{\gamma\gamma} = c_{gg} = 0$ is shown on plot (b). Finally, the four best-fit point locations are indicated by crosses in plot (c). The theoretically predicted lines for extra quarks of type b' [plots (c) and (d)] and t' [plot (b)] are also represented (red).

For the sake of generality, we consider the whole ranges of $c_{\gamma\gamma}$, c_{gg} values pointed out by the Higgs rate fits.

The $c_{t,b,\tau}$ choice is also related to the generation of fermion masses through Yukawa couplings. In the SM, the top quark mass determines Y_t up to Cabibbo-Kobayashi-Maskawa mixing angles. For large deviations with respect to the SM Yukawa coupling, i.e., for c_t values very different from unity, the physical top mass may be recovered by new strong mixing effects like in t - t' mixings. $|c_t|$ values different from unity by a factor ~ 5 would certainly already require strong t - t' mixings to be predicted

by specific scenarios. Similar comments hold for c_b and c_τ . From this point of view, the value of $c_b = 10$ in Fig. 1(d) and $c_\tau = 0.05$ in Fig. 2(a) are respectively large and tiny; those have been chosen for the purpose of explaining the behavior of the best-fit domains in the large c_b and low c_τ regimes.

2. Best-fit points

The best-fit points reachable when varying the three free parameters c_b , c_{gg} , $c_{\gamma\gamma}$, for fixed values $c_t = 1$ and $c_\tau = 1$,

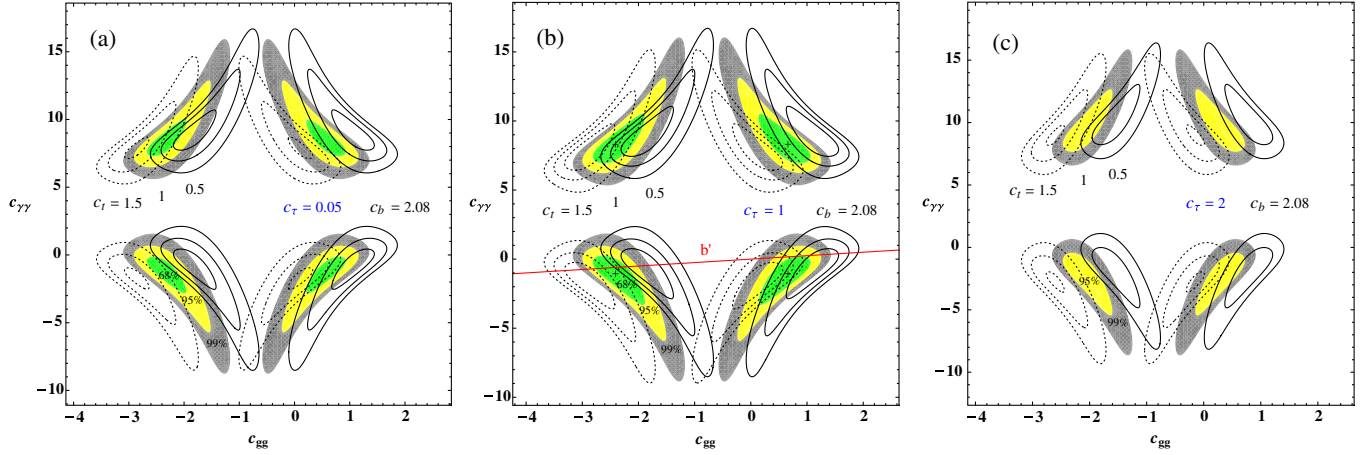


FIG. 2 (color online). Best-fit regions at 68.27% C.L. (green), 95.45% C.L. (yellow) and 99.73% C.L. (grey) in the plane $c_{\gamma\gamma}$ versus c_{gg} , for $c_b = 2.08$. Each one of the three figures is obtained for a c_τ value which is indicated in blue. In each figure, the regions are drawn for three c_τ values (same conventions as in Fig. 1). The predicted (red) line for an extra quark of type b' is also represented in plot (b).

are at $c_b = 2.08$ and the c_{gg} , $c_{\gamma\gamma}$ values corresponding to the four crosses drawn in Fig. 1(c). Since there are exact symmetries along the c_{gg} and $c_{\gamma\gamma}$ axes (see discussion below), those four cross points are all associated to the same $\chi^2_{\min} = 52.36$.

For comparison, the best-fit point reachable when varying the five effective parameters c_t , c_b , c_τ , c_{gg} , $c_{\gamma\gamma}$ is $\{c_t = 0.0; c_b = 1.13; c_\tau = 0.0; c_{gg} = -0.79; c_{\gamma\gamma} = -0.11\}$ leading to $\chi^2 = 50.26$. A vanishing c_t (a top-phobic Higgs boson) imposes $\mu_{7,\text{CMS}}^{VI} = 0$ [via Eq. (6)] which lies inside the 1σ experimental interval and is even the possible value closest to the measured negative central value [given just after Eq. (11)]. Similarly, $c_\tau = 0$ (tau phobic) induces $\mu_{7/8,\text{CMS}}^{XII} = 0$ which is the closest value to the negative experimental central values. In view of the generation of fermion masses through the Yukawa couplings, one could require say $|c_\tau| > 0.3$ and $|c_t| > 0.3$ which lead instead to the best-fit point $\{c_t = 0.3; c_b = 1.18; c_\tau = -0.3; c_{gg} = 0.67; c_{\gamma\gamma} = -0.42\}$ having $\chi^2 = 50.44$.

All these minimal χ^2 values are smaller than the SM one, $\chi^2_{\text{SM}} = 57.10$ [from taking all the strength predictions at unity in Eq. (12)]. The regions at 68.27% C.L. in Fig. 1(b) do not even contain the SM point $\{c_t = 1; c_b = 1; c_\tau = 1; c_{gg} = 0; c_{\gamma\gamma} = 0\}$.

Let us interpret the c values of the best-fit points obtained in Fig. 1(c) [or equivalently Fig. 2(b)]. For example, the best-fit point at $c_b = 2.08$, $c_{gg} = 0.66$ and $c_{\gamma\gamma} = -1.09$ shown in Fig. 1(c) (for fixed $c_t = c_\tau = 1$) indicates in particular that an increase of the diphoton partial width is favored by the data. Indeed, a negative $c_{\gamma\gamma}$ implies a constructive interference between EF loops and the main SM W^\pm -boson exchange, as Eq. (5) shows. Interestingly, the preferred $c_{\gamma\gamma}$ value approximatively cancel the top-loop contribution. The obtained indication for a

$\Gamma_{h \rightarrow \gamma\gamma}$ enhancement is not surprising as most of the measured strengths in the diphoton channel—described in Sec. III—are above their SM expectations (even significantly for some of those).

The best-fit value $c_{gg} = 0.66$ also outlines the preference for a $\sigma_{gg \rightarrow h}$ increase [see Eq. (4)] related to the excesses with respect to the SM rates of the experimental values for some of the diphoton rates.

Finally, a $\Gamma_{h \rightarrow b\bar{b}}$ increase is favored [see Eq. (6) with $c_b = 2.08$] which tends to enhance the $\mu_{1.96,\text{CDF+D0}}^V$ strength and suppress $\mu_{7/8,\text{CMS}}^{XII}$ relatively to the SM, as indicated by the experimental results (all at more than 1σ from the SM).

The three other best-fit points of Fig. 1(c) can be obtained through the symmetries described in the next subsection and are thus interpretable with the same physical arguments about the Higgs rates.

3. The symmetries

Some exact reflection symmetries with respect to vertical and horizontal axes appear clearly in Figs. 1 and 2. Indeed, for a $c_{\gamma\gamma}$ value giving rise to a certain $\Delta\chi^2$, there always exists a $c_{\gamma\gamma}$ partner value leading to the opposite-sign $h \rightarrow \gamma\gamma$ amplitude [squared in Eq. (5)] and in turn to the same $\Delta\chi^2$. The same kind of symmetry occurs for c_{gg} entering the $h \rightarrow gg$ (or $gg \rightarrow h$) amplitude.

Another type of symmetry is constituted by the transformation $c_b \rightarrow -c_b$ leaving invariant the $b\bar{b}$ partial width [cf. Eq. (6)]. This symmetry is approximative due to the dependence of $\sigma_{gg \rightarrow h}$ and $\Gamma_{h \rightarrow \gamma\gamma}$ on c_b ; for c_b values such that the bottom-exchange contributions to $\sigma_{gg \rightarrow h}$ and $\Gamma_{h \rightarrow \gamma\gamma}$ remain subleading (as in the SM), the transformation $c_b \rightarrow -c_b$ keeps unchanged, at the percent level, the

$c_{\gamma\gamma}$, c_{gg} values associated to a given $\Delta\chi^2$. The similar symmetry arises for $c_\tau \rightarrow -c_\tau$.

4. Dependence of the best-fit regions on c_{gg} and $c_{\gamma\gamma}$

At this level, one is able to interpret the typical shapes of the obtained best-fit regions. The typical oblique direction (diagonal positioning) of the best-fit domains, for example for the fixed value $c_t = 1$, around the best-fit point at $c_{gg} = 0.66$ and $c_{\gamma\gamma} = -1.09$ in Fig. 1(c), can be understood as follows: the orientations of the three other best-fit region groups are then deduced through the reflection symmetries along c_{gg} and $c_{\gamma\gamma}$. Starting from this best-fit point and decreasing c_{gg} tends to decrease $\sigma_{gg\rightarrow h}$ and hence to degrade the fits for diphoton rates, a degradation which must be compensated by the $c_{\gamma\gamma}$ decrease ($|c_{\gamma\gamma}|$ increase enhancing $\Gamma_{h\rightarrow\gamma\gamma}$) to remain below 68.27% C.L.

5. Dependence of the best-fit regions on c_t

We discuss now the modifications of the best-fit domains as the effective parameter c_t is varying. We observe separately on Figs. 1(a)–1(c) and 2 that a c_t variation of amount δc_t leads in a good approximation to a translation (no domain shape modification) of $-\delta c_t$ along both the $c_{\gamma\gamma}$ and c_{gg} axes for each one of the three best-fit regions. It is particularly clear in Fig. 1(b) where a large δc_t is exhibited.

Indeed, considering a given confidence level, the $\Delta\chi^2 = \chi^2 - \chi_{\min}^2$ value is fixed which determines [cf. Eq. (12)] in particular the c_t correction factor for the major top loop exchanges and the parameters for EF loop contributions c_{gg} , $c_{\gamma\gamma}$ entering the predicted strengths [cf. Eq. (10)] through the sums $(c_t + c_{gg})$ and $(c_t + c_{\gamma\gamma})$ [cf. Eqs. (4) and (5)]. Hence for a δc_t parameter variation, since the χ_{\min}^2 value is unchanged (for similar compensation reasons to the following one), the induced χ^2 modification should be exactly compensated by variations $\delta c_{gg} = \delta c_{\gamma\gamma} = -\delta c_t$.

Note that for different c_t , c_{gg} and $c_{\gamma\gamma}$ definitions from here (then distinguished by a prime), say generalizing to effective parameters entering Eqs. (4) and (5) via $(\alpha_g c'_t + \beta_g c'_{gg})$ and $(\alpha_\gamma c'_t + \beta_\gamma c'_{\gamma\gamma})$ with new constants $\alpha_{g,\gamma}$, $\beta_{g,\gamma}$, the translations would be instead of

$$\delta c'_{gg} = -\frac{\alpha_g}{\beta_g} \delta c'_t \quad \text{and} \quad \delta c'_{\gamma\gamma} = -\frac{\alpha_\gamma}{\beta_\gamma} \delta c'_t.$$

The measured signal strength of Eq. (11) is also sensitive to c_t^3 and there is no possible δc_t compensation in it, as Eq. (6) shows, which invalidates the above argumentation strictness. Nevertheless, since the error bar on this

³Other signal strengths, like in the diphoton channel, are also sensitive to c_t [cf. Eq. (10)] but less, due to the experimental selection efficiencies and the smallness of $\sigma_{\text{h}\bar{\text{t}}}$ relatively to the dominant Higgs production reactions.

measured rate is quite large, the above translation estimations remain a good approximation up to relatively large $|c_t|$ values where the three reference best-fit domain sizes start to decrease before disappearing. This is visible for instance in Fig. 1(d); in fact these more central, i.e., more fit-favored domains in the $\{c_{\gamma\gamma}, c_{gg}\}$ plane mainly allow us to balance the degradation of the $\mu_{7,\text{CMS}}^{\text{VI}}$ fit due to larger $|c_t|$ values (tending to increase too much the $\text{h}\bar{\text{t}}$ production cross section). This effect of decreasing domain widths appears in Fig. 1(d) for smaller $|c_t|$ values than in all the other figures because for this extremely large $c_b = 10$ enhancing $B_{\text{h}\rightarrow\text{b}\bar{\text{b}}}$, $\mu_{7,\text{CMS}}^{\text{VI}}$ is getting above its 1σ range faster as $|c_t|$ increases.

To conclude on this part, this strong parameter interdependence implies that in order to determine experimentally the $c_{\gamma\gamma}$ and c_{gg} quantities, it is crucial to determine as well the c_t Yukawa correction whose measurement is essentially relying on the μ^{VI} analysis. Now this analysis requires in particular good efficiencies for the challenging simultaneous reconstruction of the top and bottom quark pairs in the final state.

6. Dependence of the best-fit regions on c_b

Concerning the c_b variation (for fixed $c_t = c_\tau = 1$), we first explain the impact of the c_b increase on the typically allowed $c_{\gamma\gamma}$, c_{gg} values starting from the best-fit domains around the best-fit point $\{c_b = 2.08; c_{gg} = 0.66; c_{\gamma\gamma} = -1.09\}$ in Fig. 1(c) and the reasons why huge values up to $c_b \approx 50$ could still agree with present Higgs rate fits. For such a c_b increase, the strengths $\mu_{7/8,\text{ATLAS/CMS}}^{\text{VII,VIII}}$, $\mu_{1.96,\text{CDF+D0}}^{\text{XI}}$ and $\mu_{7/8,\text{CMS}}^{\text{XIV}}$ are reduced via $\Gamma_{\text{h}\rightarrow\text{b}\bar{\text{b}}}$, a reduction which has to be compensated by a $\sigma_{gg\rightarrow h}$ increase through a c_{gg} enhancement to conserve a satisfactory χ^2 (or equivalently here, $\Delta\chi^2$). This explains the shift of the considered best-fit domains, around $\{c_b = 2.08; c_{gg} = 0.66; c_{\gamma\gamma} = -1.09\}$ in Fig. 1(c), to higher c_{gg} values in Fig. 1(d) where $c_b = 10$ (still with $c_t = 1$). This necessary compensation between the $\Gamma_{\text{h}\rightarrow\text{b}\bar{\text{b}}}$ and $\sigma_{gg\rightarrow h}$ increases also guarantees the stability of diphoton rates (there is also a significant gluon-gluon fusion contribution in the three dijet-tagged final states) letting the χ^2 at the same level, without $c_{\gamma\gamma}$ modifications—explaining nearly identical $c_{\gamma\gamma}$ values for the studied regions in Figs. 1(c) and 1(d). The $\Gamma_{\text{h}\rightarrow\text{b}\bar{\text{b}}}$ increase leads to enhancements of the strengths $\mu_{7/8,\text{ATLAS/CMS}}^{\text{IV}}$, $\mu_{1.96,\text{CDF+D0}}^{\text{V}}$ and $\mu_{7,\text{CMS}}^{\text{VI}}$ without major consequences on the fit; a c_b increase up to ~ 50 (leading to $\Gamma_{\text{h}\rightarrow\text{b}\bar{\text{b}}} \lesssim 5$ GeV) would still leave existing domains at 68.27% C.L. since in the theoretical limit $c_b \rightarrow \infty$, $B_{\text{h}\rightarrow\text{b}\bar{\text{b}}}$ tends obviously to a finite value compatible with the data: $B_{\text{h}\rightarrow\text{b}\bar{\text{b}}} \rightarrow 1$. Similarly, the $\Gamma_{\text{h}\rightarrow\text{b}\bar{\text{b}}}$ induced decrease of $\mu_{7/8,\text{CMS}}^{\text{IX,X,XII,XIII}}$ does not affect significantly the global fit; in the limit $c_b \rightarrow \infty$, all these signal strengths tend to zero (via the involved branching ratios) which is clearly in

agreement at 1σ with their experimental central value (and $\mu_{7/8,\text{CMS}}^{XII}|_{\text{exp}}$ is negative).

There is another effect induced by the c_b enhancement: as c_b is increasing, its contribution to $\sigma_{\text{gg}\rightarrow\text{h}}$ renders softer the $\sigma_{\text{gg}\rightarrow\text{h}}$ evolution with c_{gg} so that the c_{gg} interval spanning the $\sigma_{\text{gg}\rightarrow\text{h}}$ range allowed by the fit gets larger. This can be seen by comparing the considered best-fit domain widths along the c_{gg} axis in Figs. 1(c) and 1(d).

Now in the other direction, when c_b decreases from its value in Fig. 1(c) down to its values in Fig. 1(b) and finally Fig. 1(a), the dominant effect of surface area diminution (and disappearance) for the best-fit regions is related to $\mu_{1.96,\text{CDF}+\text{D0}}^{\text{V}}$ which is reduced and thus moved away from its best-fit value.

What is the experimental impact of the above c_b variation analysis?—The present experimental results do not prevent c_b from taking extremely large values, due in particular to Higgs rate compensations. In order to put a more stringent experimental upper limit on it, one could of course if possible improve the accuracies on the signal strengths involving $\sigma_{\text{gg}\rightarrow\text{h}}$ and $\Gamma_{\text{h}\rightarrow\text{bb}}$. A new possibility to measure c_b (or equivalently the bottom Yukawa coupling constant) would be to investigate the processes $\bar{q}q \rightarrow \text{hbb}$ and $\text{gg} \rightarrow \text{hbb}$ (or $\text{bb} \rightarrow \text{h}$ and $\text{bg} \rightarrow \text{hb}$) followed by the decay $\text{h} \rightarrow \text{bb}$. Indeed, here both the production and decay rates should increase with c_b ($\Gamma_{\text{h}\rightarrow\text{bb}}$ being the dominant partial width) so that compensations should not occur; then too large c_b values would be experimentally ruled out. This Higgs production in association with bottom quarks could have significant cross sections for high LHC luminosities and enhanced c_b values compared to the SM [102] as the present fit points out. The sensitivity to such a reaction relies deeply on the b-tagging capability [87]. This reaction suffers from large QCD backgrounds but new search strategies have been developed for such a bottom final state topology, as in Ref. [103].

7. Dependence of the best-fit regions on c_τ

Finally, to complete our discussion on the parameter variations, we describe the c_τ influence on the best-fit domains. If the fixed c_τ parameter is chosen at a larger value, like in Fig. 2(c) compared to Fig. 2(b), the induced best-fit c_b value obtained by χ^2 minimization is modified. The best-fit $\mu_{7/8,\text{CMS}}^{XII}$ value minimizing χ^2 can involve (via $B_{\text{h}\rightarrow\tau\tau}$) a larger best-fit c_b value in the case of Fig. 2(c) than in the case of Fig. 2(b) to compensate the higher c_τ (also entering $B_{\text{h}\rightarrow\tau\tau}$). Consequently, along the c_b axis, the distance of the regions in Fig. 2(c) (at $c_b = 2.08$) to the best-fit point at $c_b > 2.08$ is larger than the distance of the domain slices in Fig. 2(b) (also at $c_b = 2.08$) to the best-fit point at $c_b = 2.08$ [indicated by the cross(es) on the figure]. Along the $c_{\gamma\gamma}$ and c_{gg} axes, the typical distances of contours at a given confidence level to the respective central best-fit points are shorter in Fig. 2(c) than in

Fig. 2(b). In other terms, best-fit regions in Fig. 2(c) are smaller than in Fig. 2(b).

The c_τ decrease from Fig. 2(b) to 2(a) leads to a softer region size reduction (in the limit $c_\tau \rightarrow 0$, $\mu_{7/8,\text{CMS}}^{XII} \rightarrow 0$ which is the preferred strength).

C. The case of single EF scenarios

In this section, we apply the constraints from the Higgs rate fit to examples of simple scenarios where a unique EF state significantly affects the Higgs interactions.

1. An EF mixed with SM fermions

For instance, a single b' state (same color representation and electromagnetic charge as the bottom quark) that could be a light custodian top partner in warped/composite frameworks, would lead to a ratio in Eq. (9) $(c_{\gamma\gamma}/c_{\text{gg}})|_{b'} = 1/4$ corresponding to the straight line drawn on Figs. 1(c) and 1(d). Generically, a b' would be mixed with the SM bottom quark so that possibly $c_b \neq 1$, whereas one would have $c_t = c_\tau = 1$, like in Figs. 1(c) and 1(d). These figures show that there exist $c_{\gamma\gamma}$, c_{gg} and c_b values for which the predicted b' line crosses the 68.27% C.L. region. The simultaneous knowledge of the exact position on the b' line and the c_b value fixing the C.L. regions necessary to determine the goodness of fit requires the specification of the bottom mass matrix and hence of the considered model.

The other example of an EF candidate that is able to be mixed with SM quarks is the t' state, possibly constituted e.g., by a light top partner in little Higgs models. For a dominant t' state, the ratio of Eq. (9) tends to one which corresponds to the straight line on Fig. 1(b). Since a t' field can mix with the top quark, $c_t \neq 1$, but in the context of a single t' one should have $c_b = c_\tau = 1$ as in Fig. 1(b). The predicted t' line crosses two 95.45% C.L. regions e.g., for $c_t = 0.5$, as well as two 68.27% C.L. regions exclusively in the range $c_t \sim 1.1 \leftrightarrow 2.6$ (above ~ 2.6 the region sizes decrease as explained in Sec. IV B 5).

These discussions on the b' and t' states illustrate the fact that it is useful to study the best-fit domains in the $\{c_{\gamma\gamma}, c_{\text{gg}}\}$ plane as, in simplified models, the theoretical prediction for the $c_{\gamma\gamma}/c_{\text{gg}}$ ratio takes a simple form independent of the extra-quark masses and Yukawa couplings.

For a single extra lepton (colorless) with charge $Q_{\ell'} = -1$ potentially mixed with the SM τ lepton, the parameters $c_b = c_t = 1$, $c_{\text{gg}} = 0$ [see Eq. (7)] are fixed and there remain two free effective parameters, namely $c_{\gamma\gamma}$ and c_τ . The best-fit regions for such a two-dimensional fit are presented in Fig. 3. The two best-fit points shown in this figure correspond to $\chi_{\text{min}}^2 = 52.54$.

2. An EF unmixed with SM fermions

It is also possible theoretically that the new single t' (or b') particle does not mix with the SM top (bottom) quark. This would be the case as well for additional q' quarks with

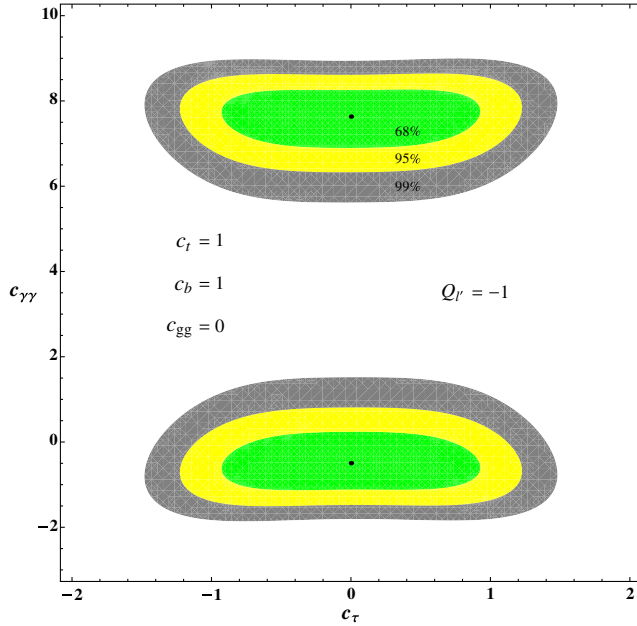


FIG. 3 (color online). Best-fit regions at 68.27% C.L., 95.45% C.L. and 99.73% C.L. in the plane $c_{\gamma\gamma}$ versus c_τ , for the case of an extra lepton with electric charge $Q_{l'} = -1$ corresponding to $c_t = c_b = 1$, $c_{gg} = 0$. The two best-fit points are indicated in black.

exotic electric charges. For illustration, let us first concentrate on the components of possible extensions of the SM quark multiplets under $SU(2)_L$, as in warped/composite frameworks where SM multiplets are promoted to representations of the custodial symmetry [63–74]. The charges for such q' components obey the relation $\mathcal{Y}_{q'} = Q_{q'} - I_{3L}^{q'}$ [$\mathcal{Y} \equiv$ hypercharge, $I_{3L} \equiv SU(2)_L$ isospin]. We will consider the electric charges of smallest absolute values $Q_{q'} = -1/3, 2/3, -4/3, 5/3, -7/3$ and $8/3$, keeping in mind that the naive perturbative limit on the electric charge reads as $|Q_{q'}| \lesssim \sqrt{4\pi/\alpha} \simeq 40$ ($\alpha \equiv$ fine-structure constant [88]). The q' states are in the same color representation as the SM quarks.

In the case of the presence of such a q' quark unmixed with SM quarks, while $c_t = c_b = c_\tau = 1$, one has $c_{\gamma\gamma} \neq 0$ and $c_{gg} \neq 0$ if the q' state possesses nonzero Yukawa couplings; the best-fit domains for a two-dimensional fit keeping the fixed parameters $c_t = c_b = c_\tau = 1$ are shown in Fig. 4 together with the four best-fit points associated to $\chi_{\min}^2 = 55.04$. On this plot, we also represent the theoretically predicted regions in the cases of a single q' quark with electric charge $Q_{q'}$: these regions are the straight lines defined by Eq. (9). All the predicted lines—whatever is the $Q_{q'}$ charge—cross the SM point which is reached in the decoupling limit $c_{\gamma\gamma} \rightarrow 0$, $c_{gg} \rightarrow 0$. The first result is that the upper-left best-fit regions around $c_{\gamma\gamma} \sim 8$, $c_{gg} \sim -1.8$ cannot be explored in single q' models (no line can reach it). We also observe in Fig. 4 that the predicted line being

the closest to a best-fit point is for $Q_{q'} = -7/3$. This result means that, among any possible SM multiplet extension component, the fit prefers the $q_{-7/3}$ state compared for example to a t' or $q_{5/3}$ state. For instance, this latter $q_{5/3}$ state leads to a smaller $|c_{\gamma\gamma}/c_{gg}|_{q'}$ ratio ($\propto Q_{q'}^2$) which is less favored by the data due in particular to the observed diphoton rate enhancements.

A possibility in the future is that, as the measurements of the Higgs signal strengths will improve their accuracies—leading typically to smaller best-fit regions in plots such as Fig. 4—some absolute charges, like for example, $|Q_{q'}| = 2/3$, could get excluded at 68.27% C.L. (the overlaps of the associated line with any 1σ region could disappear). This kind of exclusion would be quite powerful in the sense that it would be independent of the $Y_{q'}$ Yukawa coupling constants, the q' mass values ($m_{q'}$) and the q' representations under $SU(2)_L$. This is due to the simplifications occurring in the ratio of Eq. (9) or in other terms to the correlations between $c_{\gamma\gamma}$ and c_{gg} [see Eqs. (7) and (8)].

Best-fit domains in the plane of the Yukawa coupling versus the EF mass.—Now we determine the physical parameters corresponding typically to an overlap between a given line in Fig. 4 and the best-fit regions; we consider the characteristic examples of the charges $Q_{q'} = -1/3, 5/3$ and $8/3$. More precisely, we plot in Fig. 5 the regions in the plane $|m_{q'}|$ versus $\tilde{Y}_{q'} = -Y_{q'}/\text{sign}(m_{q'})$ which

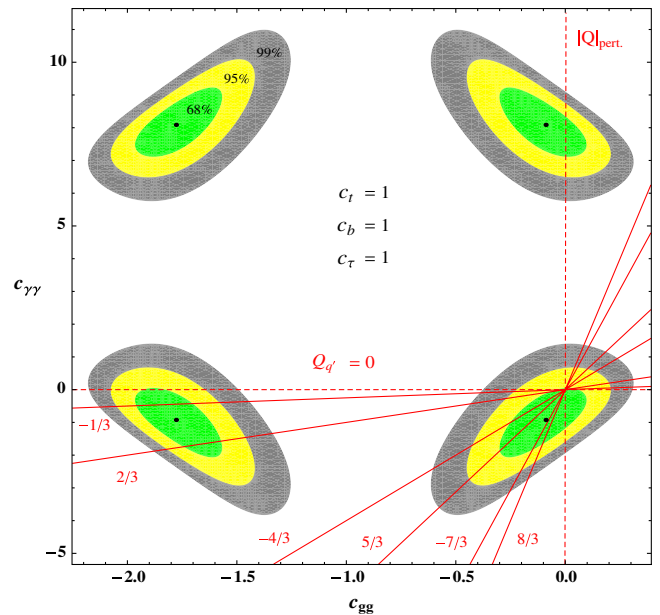


FIG. 4 (color online). Best-fit regions at 68.27% C.L., 95.45% C.L. and 99.73% C.L. in the plane $c_{\gamma\gamma}$ versus c_{gg} , for $c_t = c_b = c_\tau = 1$. Also represented are the predicted (red plain) lines for extra quarks with the several electric charges $Q_{q'} = -1/3, 2/3, -4/3, 5/3, -7/3$ and $8/3$. The extreme (red dashed) lines for $Q_{q'} = 0$ and $|Q_{q'}| = |Q_{q'}|_{\text{pert}} = \sqrt{4\pi/\alpha}$ are shown as well. The four best-fit points are indicated in black.

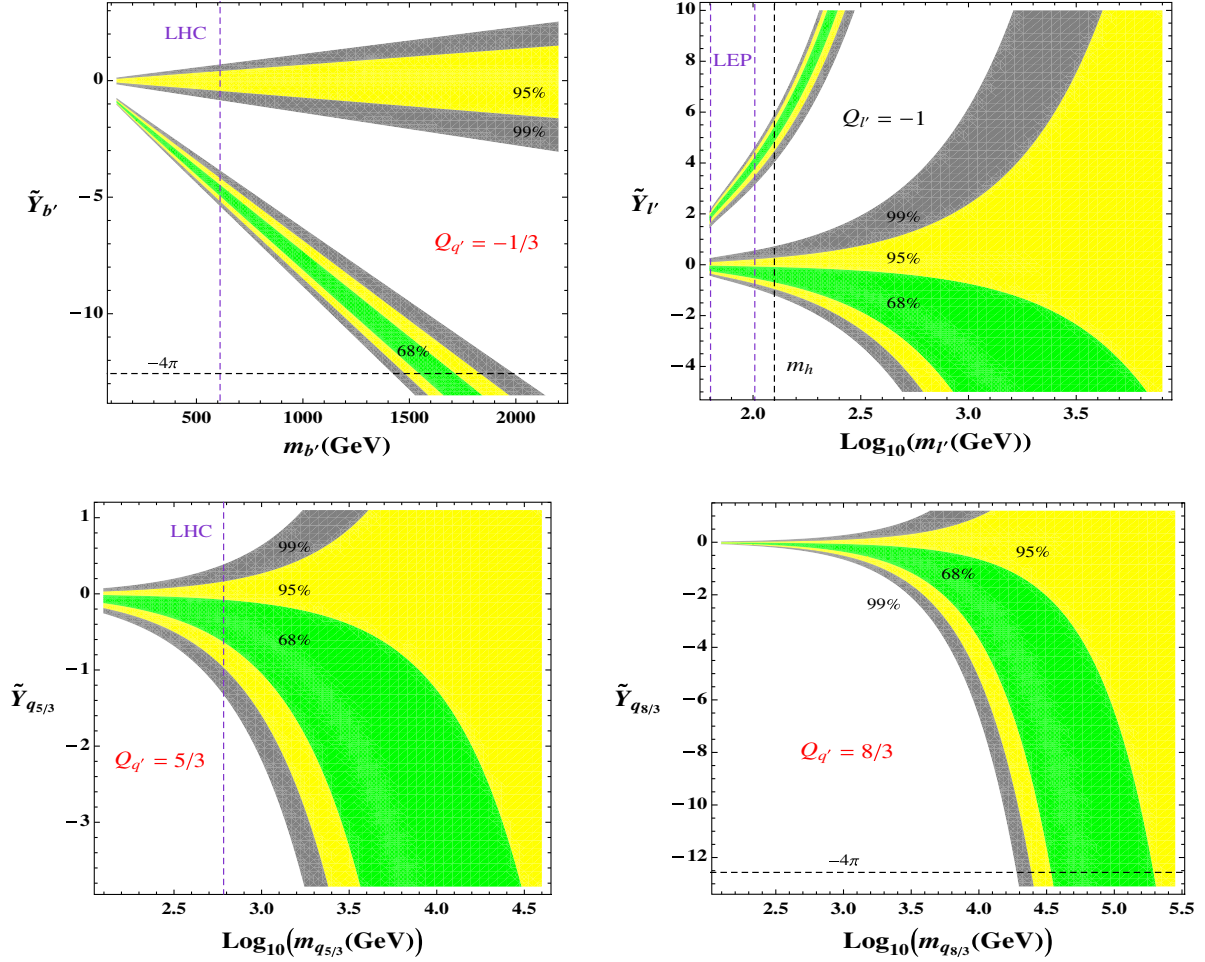


FIG. 5 (color online). Best-fit regions at 68.27% C.L., 95.45% C.L. and 99.73% C.L. in the plane of the $|m_{f'}$ absolute mass (in GeV) versus the $\tilde{Y}_{f'}$ coupling, with $c_t = c_b = c_\tau = 1$, for the cases $Q_{q'} = -1/3, 5/3, 8/3$ and $Q_{l'} = -1$. Also represented as dashed lines are the lower perturbative limit on Yukawa couplings -4π (black horizontal lines), and the direct LHC bounds $m_{b'} > 611$ GeV, $m_{q_{5/3}} > 611$ GeV, or LEP constraint $m_{l'} > 63.5$ GeV (> 101.9 GeV) for $m_{l'} - m_{\nu'} > 7$ GeV (> 15 GeV) (purple vertical lines). The mass ranges start at the Higgs mass m_h (see Footnote ¹), except for the ℓ' -lepton case (see text) where the m_h value is indicated by a black dashed vertical line.

correspond [see Eqs. (7) and (8)] to $c_{\gamma\gamma}$, c_{gg} quantities giving rise to the best $\Delta\chi^2$ values in the case of one free effective parameter, say c_{gg} (related to $c_{\gamma\gamma}$ through the fixed ratio $c_{\gamma\gamma}/c_{gg}|_{q'} \propto Q_{q'}^2$).

In Fig. 5, we also illustrate the case of a single additional ℓ' lepton (colorless) without significant mixing to SM leptons [$c_\tau = 1$], as may be justified by exotic $Q_{\ell'}$ charges or the large mass difference between the SM and extra leptons. Here we choose $Q_{\ell'} = -1$ being quite common for extra-lepton scenarios (as for instance recently in Ref. [81]). There is, again, a unique free effective parameter $c_{\gamma\gamma}$ since $c_{gg} = 0$.

Let us discuss the results shown in Fig. 5. For a given confidence level, the linear dependence of $\tilde{Y}_{b'}$ on $|m_{b'}|$ appearing clearly on the upper-left plot is explained by the expressions (7) and (8) and the constant limit $A[\tau(m_{b'} \gg m_h)] \rightarrow 1$ [described after Eq. (3)]. This linear

behavior also holds for the three other cases illustrated in this figure, even if for those it is hidden by the chosen logarithmic scale (allowing for a better view of the couplings in the small mass ranges). Equations (7) and (8) show that increasing $Q_{q'}$ leads to a slower evolution of $|\tilde{Y}_{q'}|$ with $|m_{q'}|$ (perturbative limit -4π , reached for higher $|m_{q'}|$) and a smaller allowed $\tilde{Y}_{q'}$ range at fixed $|m_{q'}|$ as can be observed by comparing $Q_{q'} = 5/3$ and $8/3$ in Fig. 5. Comparing a ℓ' extra lepton with the b' extra quark, it appears in Eq. (8) that the smaller $N_c^{\ell'} = 1$ color number tends to compensate the larger $Q_{\ell'}^2 = 1$ squared charge (the favored $c_{\gamma\gamma}|_{f'}$ interval size also affects the $\tilde{Y}_{f'}$ range width). The two unconnected 95.45% C.L. regions in the $\{|m_{b'}|, \tilde{Y}_{b'}\}$ plane correspond basically to the two overlaps between the 95.45% C.L. domains and the b' line in Fig. 4.

We now describe the direct experimental constraints indicated on the various plots of Fig. 5. The LHC bound

$m_{b'}$ > 611 GeV illustrated on the upper-left plot is the strongest direct experimental constraint on a b' state; this bound is based on the QCD b' pair production and it is less stringent for a branching ratio $B_{b' \rightarrow tW^-} < 1$ [104]. The bound for $B_{b' \rightarrow tW^-} = 1$ combined with the 68.27% C.L. region push the Yukawa couplings towards large absolute values, as Fig. 5 is demonstrating. The experimental bounds from investigations of other decay channels like $b' \rightarrow bZ$ or $b' \rightarrow bh$ are not relevant in the context of a b' field unmixed with SM quarks. The bound $m_{q_{5/3}} > 611$ GeV from the LHC shown in Fig. 5 is imposed by the search for the same decay final state $q_{5/3} \rightarrow tW^+$ following the $q_{5/3}$ pair production; this bound is obtained for $B_{q_{5/3} \rightarrow tW^+} = 1$ [104], and it leaves a possible region at 68.27% C.L. in Fig. 5. Concerning the $q_{8/3}$ particle which could decay as $q_{8/3} \rightarrow tW^+W^+$, there have been no experimental searches so far.

There exist bounds on extra leptons from the LEP collider; those read as $m_{\ell'} > 63.5$ GeV ($m_{\ell'} > 101.9$ GeV) for $m_{\ell'} - m_{\nu'} > 7$ GeV (> 15 GeV) [81,88], in the case of the existence of an additional ν' neutrino (which would have no effects on the Higgs couplings to charged fermions or gauge bosons). These constraints have been obtained from investigating the channel $\ell' \rightarrow W^{(*)}\nu' \rightarrow \ell + \cancel{E}$, where ℓ denotes a SM charged lepton and \cancel{E} stands for missing energy, assuming a stable ν' on collider time scales. The results for the domain $m_h > m_{\ell'}$ shown in Fig. 5 are valid in the absence of new significant partial Higgs decay widths (see Footnote 1).

To conclude on all these aspects of Fig. 5, one can say that the collider constraints from Higgs rate measurements on representative single EF models are already significant, especially in the low-mass regime where the allowed range for Yukawa coupling constants can be quite predictive. The constraints are sensitive to larger masses in cases of higher electric charges, as expected, and this indirect sensitivity on EF candidates can reach large mass scales up to ~ 200 TeV.

Constraints on the signs of fundamental parameters.— Concerning the constraints on the signs, as shown in Fig. 5 based on the present Higgs data, the sign $\tilde{Y}_{q'} < 0$ (leading to $c_{\gamma\gamma} < 0$) is preferred at 68.27% C.L. (except with absolute charges $|Q_{q'}| \gtrsim 7$, i.e., in a range close to the $|Q_{q'}|_{\text{pert}}$ limit as illustrated in Fig. 4) for any single extra quark as it creates a constructive interference with the W^\pm -boson exchange increasing the diphoton rates. The specific sign configuration $\tilde{Y}_{q'} < 0$ is selected by the two relevant best-fit points which pin down $c_{\gamma\gamma} < 0$, as obtained for extra quarks in Fig. 4. This predicted condition means that the Yukawa coupling constant ($-Y_{q'}$ in our conventions) must have a sign opposite to $m_{q'}$ which could be written as

$$\text{sign}\left(\frac{-Y_{q'}}{m_{q'}}\right) < 0. \quad (13)$$

Related to this condition, there are comments on the configuration denoted as *dysfermiophilia* in the literature. As described at the end of Sec. II C, strictly speaking the $c_{t,b,\tau}$ parameters entering Eqs. (4) and (5)—whose values are generally given in best-fit plots such as the present ones in Fig. 1—should in fact be understood as being

$$\begin{aligned} \epsilon_t c_t &= \frac{\text{sign}(m_t)}{\text{sign}(m_t^{\text{EF}})} c_t = \frac{\text{sign}(m_t)}{\text{sign}(m_t^{\text{EF}})} \frac{\text{sign}(-Y_t^{\text{EF}})}{\text{sign}(-Y_t)} |c_t| \\ &= \frac{\text{sign}(-Y_t^{\text{EF}})}{\text{sign}(m_t^{\text{EF}})} |c_t| = \text{sign}\left(\frac{-Y_t^{\text{EF}}}{m_t^{\text{EF}}}\right) \left|\frac{Y_t^{\text{EF}}}{Y_t}\right|, \end{aligned}$$

in our conventions of Lagrangian (1), and similarly for $\epsilon_{b,\tau} c_{b,\tau}$; here the EF exponent indicates that the parameter is considered within the context of a EF model (and remind that m_t, Y_t are in the SM). Therefore, the *dysfermiophilia* property of increasing $\Gamma_{h \rightarrow \gamma\gamma} / \Gamma_{h \rightarrow \gamma\gamma}^{\text{SM}}$ via changing the top Yukawa sign is in fact relying on the possibility to have $\epsilon_t c_t < 0$, or equivalently, $\text{sign}(-Y_t^{\text{EF}}/m_t^{\text{EF}}) < 0$. This makes sense as it is the sign of $-Y_t^{\text{EF}}/m_t^{\text{EF}}$ which has a physical meaning and appears in $\Gamma_{h \rightarrow \gamma\gamma}$ [see Eq. (8) for an analogy with the t' loop].

The other comment is that the *dysfermiophilia* possibility of having $\epsilon_t c_t < 0$ can indeed give rise to an acceptable agreement with the Higgs data [see e.g., Fig. 1(d)] but it is not necessary to achieve a good agreement (cf. Fig. 4 where $\epsilon_t c_t = 1$) since the constructive interference with the W^\pm loop increasing the diphoton rates can be realized with an EF loop inducing $c_{\gamma\gamma} < 0$.

Hence the above condition (13) can be called an *extra dysfermiophilia* as it is exactly the same as for the top quark transposed to an EF. Besides, this condition (13) leads to a decrease of $\sigma_{\text{gg} \rightarrow h} / \sigma_{\text{gg} \rightarrow h}^{\text{SM}}$ for a single EF [see Eq. (7)] through negative c_{gg} values (cf. Fig. 4). Generally speaking, an *extra dysfermiophilia* is probably easier to realize than a *dysfermiophilia* due to the potentially higher degree of freedom (allowing to decorrelate EF masses and Yukawa couplings) which can come e.g., from additional mass terms not induced by EW symmetry breaking, like KK masses.

V. CONCLUSIONS

We have learned from varying the effective parameters of the Higgs rate fit that shifts of the correction factor affecting the top quark Yukawa coupling c_t lead to translations of the best-fit domains in the $\{c_{\gamma\gamma}, c_{gg}\}$ plane ($c_{\gamma\gamma}$ and c_{gg} parametrize respectively new loop contributions to the $h\gamma\gamma$ and hgg vertex) proportional to δc_t . This means that to constrain precisely the new loop contributions to the hgg and $h\gamma\gamma$ couplings, one has to determine simultaneously the top Yukawa coupling which might be an experimental challenge.

The c_{gg} determination relies significantly on the correction factor affecting the bottom quark Yukawa coupling as

well, namely c_b for which extremely large values are not ruled out by the combination of present Higgs data; for that purpose, new Higgs reactions like $gg \rightarrow h\bar{b}b$, $h \rightarrow \bar{b}b$ would be interesting to investigate experimentally.

We have then considered the effective case of a single EF affecting the Higgs rates. It could for example be the lightest KK mode of some higher-dimensional theory and have dominant effects on collider physics; the lightest KK state effects are generically at least the strongest ones, so assuming this state to be the sole one is quantitatively a good (starting) approximation. In contrast, within theories containing several crucial EF, one could of course combine the (different) single EF effects described here and there could be compensations.

In this basic single EF framework, significant constraints have been placed on extra leptons. We have also found that the Higgs rate measurements put nontrivial constraints on $c_{\gamma\gamma}$ and c_{gg} for b' , t' states able to mix with the SM b , t quarks. Regarding unmixed EF candidates (still with the same color number as SM quarks), it is remarkable that due to the $c_{\gamma\gamma} - c_{gg}$ correlations, the Higgs fit can potentially constrain intervals of absolute electric charges independently of the $SU(2)_L$ representations, Yukawa couplings and masses for the EF. Another related result is that, among any possible components of SM quark multiplet extensions, the $q_{-7/3}$ field is the one preferred by the fit. The

Higgs rate fit also allows us to constrain significantly the EF Yukawa couplings for $m_{q'}$ values up to ~ 200 TeV, and points out at 68.27% C.L. an *extra dysfermiophilia* [condition (13)] for any single q' quark (independently of $Q_{q'}$ as long as it does not approach nonperturbative couplings).

Finally, let us note that any model with EFs predicts certain values for the parameters c_t , c_b , c_τ (c_τ : correction factor for the τ -lepton Yukawa coupling) and $c_{\gamma\gamma}$, c_{gg} [easily calculable through Eqs. (7) and (8)], which can then be located on the best-fit plots obtained in this paper in order to determine the degree of compatibility with the Higgs data. Anyone could also use the synthesized fit information contained in Fig. 4 to constrain one's extra-quark electric charge, and in Fig. 5 to study the $\{|m_{f'}|, \tilde{Y}_{f'}\}$ plane of one's single f' model.

ACKNOWLEDGMENTS

The author thanks A. Azatov, H. Bachacou, O.J.P. Éboli, J.R. Espinosa, A. Falkowski, S. Gopalakrishna, C. Grojean, V. Sanz, A. Strumia, and T. Tath for useful discussions, as well as the CERN TH-Division where this paper has been initiated. This work is supported by the “Institut Universitaire de France.” The author also acknowledges support from the ANR *CPV-LFV-LHC* under Project No. NT09-508531.

-
- [1] F. Gianotti, <http://indico.cern.ch/conferenceDisplay.py?confId=197461> (2012).
 - [2] J. Incandela, <http://indico.cern.ch/conferenceDisplay.py?confId=197461> (2012).
 - [3] F. Englert and R. Brout, *Phys. Rev. Lett.* **13**, 321 (1964).
 - [4] P. W. Higgs, *Phys. Lett.* **12**, 132 (1964).
 - [5] P. W. Higgs, *Phys. Rev. Lett.* **13**, 508 (1964).
 - [6] G. Guralnik, C. Hagen, and T. Kibble, *Phys. Rev. Lett.* **13**, 585 (1964).
 - [7] ATLAS Collaboration, <https://twiki.cern.ch/twiki/bin/view/AtlasPublic> (2012).
 - [8] CMS Collaboration, <https://twiki.cern.ch/twiki/bin/view/CMSPublic/PhysicsResults> (2012).
 - [9] M. S. Carena, E. Ponton, J. Santiago, and C. E. M. Wagner, *Nucl. Phys.* **B759**, 202 (2006).
 - [10] M. Gogberashvili, *Int. J. Mod. Phys. D* **11**, 1635 (2002).
 - [11] L. Randall and R. Sundrum, *Phys. Rev. Lett.* **83**, 3370 (1999).
 - [12] T. Gherghetta and A. Pomarol, *Nucl. Phys.* **B586**, 141 (2000).
 - [13] S. J. Huber and Q. Shafi, *Phys. Lett. B* **498**, 256 (2001).
 - [14] S. J. Huber and Q. Shafi, *Phys. Lett. B* **512**, 365 (2001).
 - [15] S. J. Huber and Q. Shafi, *Phys. Lett. B* **544**, 295 (2002).
 - [16] S. J. Huber and Q. Shafi, *Phys. Lett. B* **583**, 293 (2004).
 - [17] S. Chang, C. Kim, and M. Yamaguchi, *Phys. Rev. D* **73**, 033002 (2006).
 - [18] G. Moreau and J. Silva-Marcos, *J. High Energy Phys.* **03** (2006) 090.
 - [19] G. Moreau and J. Silva-Marcos, *J. High Energy Phys.* **01** (2006) 048.
 - [20] K. Agashe, G. Perez, and A. Soni, *Phys. Rev. D* **71**, 016002 (2005).
 - [21] K. Agashe, G. Perez, and A. Soni, *Phys. Rev. Lett.* **93**, 201804 (2004).
 - [22] K. Agashe, G. Perez, and A. Soni, *Phys. Rev. D* **75**, 015002 (2007).
 - [23] K. Agashe, A. E. Blechman, and F. Petriello, *Phys. Rev. D* **74**, 053011 (2006).
 - [24] F. del Aguila, J. Aguilar-Saavedra, B. Allanach, J. Alwall, Y. Andreev *et al.*, *Eur. Phys. J. C* **57**, 183 (2008).
 - [25] M. Raidal, A. van der Schaaf, I. Bigi, M. Mangano, Y. K. Semertzidis *et al.*, *Eur. Phys. J. C* **57**, 13 (2008).
 - [26] Y. Grossman and M. Neubert, *Phys. Lett. B* **474**, 361 (2000).
 - [27] T. Appelquist, B. A. Dobrescu, E. Ponton, and H.-U. Yee, *Phys. Rev. D* **65**, 105019 (2002).
 - [28] T. Gherghetta, *Phys. Rev. Lett.* **92**, 161601 (2004).
 - [29] G. Moreau, *Eur. Phys. J. C* **40**, 539 (2005).
 - [30] C. Bouchart, A. Knochel, and G. Moreau, *Phys. Rev. D* **84**, 015016 (2011).
 - [31] F. Goertz, U. Haisch, and M. Neubert, *Phys. Lett. B* **713**, 23 (2012).

- [32] D. B. Kaplan and H. Georgi, *Phys. Lett.* **136B**, 183 (1984).
- [33] D. B. Kaplan, H. Georgi, and S. Dimopoulos, *Phys. Lett.* **136B**, 187 (1984).
- [34] R. Contino, Y. Nomura, and A. Pomarol, *Nucl. Phys.* **B671**, 148 (2003).
- [35] K. Agashe, R. Contino, and A. Pomarol, *Nucl. Phys.* **B719**, 165 (2005).
- [36] R. Contino, L. Da Rold, and A. Pomarol, *Phys. Rev. D* **75**, 055014 (2007).
- [37] G. Burdman and L. Da Rold, *J. High Energy Phys.* **12** (2007) 086.
- [38] L. Da Rold, *J. High Energy Phys.* **02** (2011) 034.
- [39] A. Azatov and J. Galloway, *Phys. Rev. D* **85**, 055013 (2012).
- [40] C. T. Hill, *Phys. Lett. B* **266**, 419 (1991).
- [41] A. Pomarol and J. Serra, *Phys. Rev. D* **78**, 074026 (2008).
- [42] N. Arkani-Hamed, A. G. Cohen, and H. Georgi, *Phys. Lett. B* **513**, 232 (2001).
- [43] N. Arkani-Hamed, A. G. Cohen, E. Katz, A. E. Nelson, T. Gregoire, and J. G. Wacker, *J. High Energy Phys.* **08** (2002) 021.
- [44] N. Arkani-Hamed, A. Cohen, E. Katz, and A. Nelson, *J. High Energy Phys.* **07** (2002) 034.
- [45] K. Ishiwata and M. B. Wise, *Phys. Rev. D* **84**, 055025 (2011).
- [46] C. Kilic, K. Kopp, and T. Okui, *Phys. Rev. D* **83**, 015006 (2011).
- [47] V. Barger, M. Ishida, and W.-Y. Keung, *Phys. Rev. Lett.* **108**, 261801 (2012).
- [48] I. Low, J. Lykken, and G. Shaughnessy, *Phys. Rev. D* **86**, 093012 (2012).
- [49] T. Corbett, O. Eboli, J. Gonzalez-Fraile, and M. Gonzalez-Garcia, *Phys. Rev. D* **86**, 075013 (2012).
- [50] P. P. Giardino, K. Kannike, M. Raidal, and A. Strumia, *J. High Energy Phys.* **06** (2012) 117.
- [51] P. P. Giardino, K. Kannike, M. Raidal, and A. Strumia, *Phys. Lett. B* **718**, 469 (2012).
- [52] J. Ellis and T. You, *J. High Energy Phys.* **06** (2012) 140.
- [53] J. Ellis and T. You, *J. High Energy Phys.* **09** (2012) 123.
- [54] A. Azatov, R. Contino, and J. Galloway, *J. High Energy Phys.* **04** (2012) 127.
- [55] A. Azatov, R. Contino, D. D. Re, J. Galloway, M. Grassi, and S. Rahatlou, *J. High Energy Phys.* **06** (2012) 134.
- [56] M. Montull and F. Riva, *J. High Energy Phys.* **11** (2012) 018.
- [57] J. Espinosa, C. Grojean, M. Muhlleitner, and M. Trott, *J. High Energy Phys.* **05** (2012) 097.
- [58] J. Espinosa, C. Grojean, M. Muhlleitner, and M. Trott, *J. High Energy Phys.* **12** (2012) 045.
- [59] D. Carmi, A. Falkowski, E. Kuflik, T. Volansky, and J. Zupan, *J. High Energy Phys.* **10** (2012) 196.
- [60] S. Banerjee, S. Mukhopadhyay, and B. Mukhopadhyaya, *J. High Energy Phys.* **10** (2012) 062.
- [61] T. Plehn and M. Rauch, *Europhys. Lett.* **100**, 11002 (2012).
- [62] ATLAS Collaboration, Report No. CONF-2012-127, 2012 (unpublished).
- [63] K. Agashe, A. Delgado, M. J. May, and R. Sundrum, *J. High Energy Phys.* **08** (2003) 050.
- [64] K. Agashe, R. Contino, L. Da Rold, and A. Pomarol, *Phys. Lett. B* **641**, 62 (2006).
- [65] A. Djouadi, G. Moreau, and F. Richard, *Nucl. Phys.* **B773**, 43 (2007).
- [66] M. S. Carena, E. Ponton, J. Santiago, and C. E. M. Wagner, *Phys. Rev. D* **76**, 035006 (2007).
- [67] A. Djouadi, G. Moreau, and R. K. Singh, *Nucl. Phys.* **B797**, 1 (2008).
- [68] A. Djouadi and G. Moreau, *Phys. Lett. B* **660**, 67 (2008).
- [69] F. Ledroit, G. Moreau, and J. Morel, *J. High Energy Phys.* **09** (2007) 071.
- [70] C. Bouchart and G. Moreau, *Nucl. Phys.* **B810**, 66 (2009).
- [71] C. Bouchart and G. Moreau, *Phys. Rev. D* **80**, 095022 (2009).
- [72] A. Djouadi, G. Moreau, F. Richard, and R. K. Singh, *Phys. Rev. D* **82**, 071702 (2010).
- [73] S. Casagrande, F. Goertz, U. Haisch, M. Neubert, and T. Pfoh, *J. High Energy Phys.* **09** (2010) 014.
- [74] A. Djouadi, G. Moreau, and F. Richard, *Phys. Lett. B* **701**, 458 (2011).
- [75] F. del Aguila, M. Perez-Victoria, and J. Santiago, *J. High Energy Phys.* **02** (2003) 051.
- [76] J. A. Cabrer, G. von Gersdorff, and M. Quiros, *J. High Energy Phys.* **01** (2012) 033.
- [77] S. Dawson and E. Furlan, *Phys. Rev. D* **86**, 015021 (2012).
- [78] M. Carena, I. Low, and C. E. Wagner, *J. High Energy Phys.* **08** (2012) 060.
- [79] A. Azatov, O. Bondu, A. Falkowski, M. Felcini, S. Gascon-Shotkin, D. Ghosh, G. Moreau, A. Rodríguez-Marrero, and S. Sekmen, *Phys. Rev. D* **85**, 115022 (2012).
- [80] N. Bonne and G. Moreau, *Phys. Lett. B* **717**, 409 (2012).
- [81] A. Joglekar, P. Schwaller, and C. E. Wagner, *J. High Energy Phys.* **12** (2012) 064.
- [82] J. Kearney, A. Pierce, and N. Weiner, *Phys. Rev. D* **86**, 113005 (2012).
- [83] M. Voloshin, *Phys. Rev. D* **86**, 093016 (2012).
- [84] B. Batell, S. Gori, and L.-T. Wang, [arXiv:1209.6382](https://arxiv.org/abs/1209.6382).
- [85] N. Arkani-Hamed, K. Blum, R. T. D'Agnolo, and J. Fan, [arXiv:1207.4482](https://arxiv.org/abs/1207.4482).
- [86] L. G. Almeida, E. Bertuzzo, P. A. Machado, and R. Z. Funchal, *J. High Energy Phys.* **11** (2012) 085.
- [87] A. Djouadi, *Phys. Rep.* **457**, 1 (2008).
- [88] K. Nakamura *et al.* (Particle Data Group), *J. Phys. G* **37**, 075021 (2010).
- [89] G. Cacciapaglia, A. Deandrea, and J. Llodra-Perez, *J. High Energy Phys.* **06** (2009) 054.
- [90] G. Cacciapaglia, A. Deandrea, D. Harada, and Y. Okada, *J. High Energy Phys.* **11** (2010) 159.
- [91] G. Cacciapaglia, A. Deandrea, L. Panizzi, N. Gaur, D. Harada, and Y. Okada, *J. High Energy Phys.* **03** (2012) 070.
- [92] LHC Higgs Cross Section Working Group, <https://twiki.cern.ch/twiki/bin/view/LHCPhysics/CrossSections> (2012).
- [93] Tevatron New Physics Higgs Working Group, CDF Collaboration, and D0 Collaboration, [arXiv:1207.0449](https://arxiv.org/abs/1207.0449).
- [94] ATLAS Collaboration, Report No. CONF-2012-091, 2012 (unpublished).
- [95] CMS Collaboration, Report No. PAS HIG-12-015, 2012 (unpublished).
- [96] S. Chatrchyan *et al.* (CMS Collaboration), *Phys. Lett. B* **716**, 30 (2012).

- [97] G. Aad *et al.* (ATLAS Collaboration), [Phys. Lett. B **716**, 1 \(2012\)](#).
- [98] ATLAS Collaboration, Report No. CONF-2012-093, 2012 (unpublished).
- [99] CMS Collaboration, Report No. PAS HIG-12-020, 2012 (unpublished).
- [100] ATLAS Collaboration, Report No. CONF-2012-019, 2012 (unpublished).
- [101] ATLAS Collaboration, Report No. CONF-2012-098, 2012 (unpublished).
- [102] S. Dawson and P. Jaiswal, [Phys. Rev. D **81**, 073008 \(2010\)](#).
- [103] M. Carena, S. Gori, A. Juste, A. Menon, C. E. Wagner, and L.-T. Wang, [J. High Energy Phys. **07** \(2012\) 091](#).
- [104] S. Chatrchyan *et al.* (CMS Collaboration), [J. High Energy Phys. **05** \(2012\) 123](#).